

# Stream power framework for predicting geomorphic change: The 2013 Colorado Front Range flood



Steven E. Yochum<sup>a,\*</sup>, Joel S. Sholtes<sup>b,c</sup>, Julian A. Scott<sup>a</sup>, Brian P. Bledsoe<sup>d</sup>

<sup>a</sup> U.S. Forest Service, National Stream and Aquatic Ecology Center, Fort Collins, CO, USA

<sup>b</sup> Colorado State University, Department of Civil and Environmental Engineering, Fort Collins, CO, USA

<sup>c</sup> U.S. Bureau of Reclamation, Technical Services Center, Sedimentation and River Hydraulics Group, Lakewood, CO, USA

<sup>d</sup> University of Georgia, School of Environmental, Civil, Agricultural, and Mechanical Engineering, Athens, GA, USA

## ARTICLE INFO

### Article history:

Received 21 October 2016

Received in revised form 3 March 2017

Accepted 4 March 2017

Available online 08 March 2017

## ABSTRACT

The Colorado Front Range flood of September 2013 induced a diverse range of geomorphic changes along numerous stream corridors, providing an opportunity to assess responses to a large flood in a semiarid landscape. We defined six classes of geomorphic change related to peak unit stream power and valley confinement for 531 stream reaches over 226 km, spanning a gradient of channel scales and slope. Geomorphic change was generally driven by erosion of channel margins in confined reaches and by a combination of deposition and erosion in unconfined reaches. The magnitude of geomorphic change typically increased with unit stream power ( $\omega$ ), with greater responses observed in unconfined channels. Cumulative logit modeling indicated that total stream power or unit stream power, unit stream power gradient, and valley confinement are significant predictors of geomorphic response for this flood event. Based on this dataset, thresholds for geomorphic adjustment were defined. For channel slopes < 3%, we noted a credible potential for substantial channel widening with  $\omega > 230 \text{ W/m}^2$  (16 lb/ft-s; at least 10% of the investigated sites experienced substantial channel widening) and a credible potential for avulsions, braiding, and loss of adjacent road embankments associated with  $\omega > 480 \text{ W/m}^2$  (33 lb/ft-s; at least 10% of the investigated sites experienced such geomorphic change). Infrequent to numerous eroded banks were very likely with  $\omega > 700 \text{ W/m}^2$  (48 lb/ft-s), with substantial channel widening or major geomorphic change shifting from credible to likely. Importantly, in reaches where there were large reductions in  $\omega$  as the valley form shifted from confined to relatively unconfined, large amounts of deposition-induced, reach-scale geomorphic change occurred in some locations at relatively low  $\omega$ . Additionally, alluvial channels with slopes > 3% had greater resistance to geomorphic change, likely caused by armoring by larger bed material and increased flow resistance from enhanced bedforms. Finally, we describe how these results can potentially be used by practitioners for assessing the risk of geomorphic change when evaluating current or planned conditions.

Published by Elsevier B.V.

## 1. Introduction

Predicting the settings where geomorphic change can be expected as a result of flooding is valuable for informing environmental management and policy, as well as specific project designs. Human encroachments into stream corridors, including roadway and railroad alignments, commercial developments, and private residences, are key drivers of flood hazards. Geomorphic change and subsequent flood hazards include localized streambank erosion, hillslope and terrace failure, reach-scale channel widening, sediment deposition and associated loss of channel and floodplain capacity, rapid downstream meander migration, and channel avulsions and braiding. Where allowed by the valley form, sufficient floodplain extent and connectivity is needed to diminish

the effects of erosive forces on streambanks, floodplain and terrace surfaces, infrastructure and property, and riparian and aquatic habitats. The identification of hydraulic thresholds beyond which a substantial potential exists for geomorphic change of channel and floodplain form are consequently quite valuable, but hindered by variability in driving mechanisms (peak discharge, flow duration, channel and floodplain slope, stream power, etc.) and resisting mechanisms (flow resistance, bank composition, vegetation type and extent, rip rap, etc.).

The 2013 Colorado Front Range flood provides an opportunity to assess geomorphic changes associated with a large flood in a semiarid landscape. This event, which impacted a substantial geographic extent and numerous streams in and adjacent to the Colorado Front Range foothills, allows us to relate diverse geomorphic changes to unit stream power ( $\omega$ ) and other variables. Observed responses ranged from undetectable or minimal impacts upon cross sections and planforms to major

\* Corresponding author.

E-mail address: [stevenyochum@fs.fed.us](mailto:stevenyochum@fs.fed.us) (S.E. Yochum).

changes including widening, braiding, overwhelming erosion of road embankments, hillslopes and terraces, and extensive aggradation. Numerous avulsions were also observed. Additionally, a large number of landslides and debris flows occurred (>1100; *Coe et al., 2014*), contributing large point sources of sediment and water to many of the most-impacted streams. The largest rainfall accumulations were observed on the mid-elevation foothills (elevations primarily from 2000 to 3000 m; *Fig. 1*). The flood response extended from confined, high-gradient reaches within canyons of the foothills to wide and lower-gradient high plains stream valleys; thus, the geomorphic variability and extent of affected reaches provide a valuable opportunity to explore relationships between hydraulic descriptors such as  $\omega$  and observed geomorphic changes.

Given the limited available guidance for predicting varying types and degrees of geomorphic change resulting from large floods, we initiated a project with the following objectives:

- develop an ordinal classification scheme describing diverse types of geomorphic change and apply it to stream reaches impacted to varying degrees by the 2013 Front Range flood;
- assess reach-specific hydraulic variables that quantify driving mechanisms of geomorphic change and assess their effectiveness for predicting observed responses; and
- identify  $\omega$  thresholds associated with specific types of geomorphic change and compare these results to previously published findings from floods in other regions.

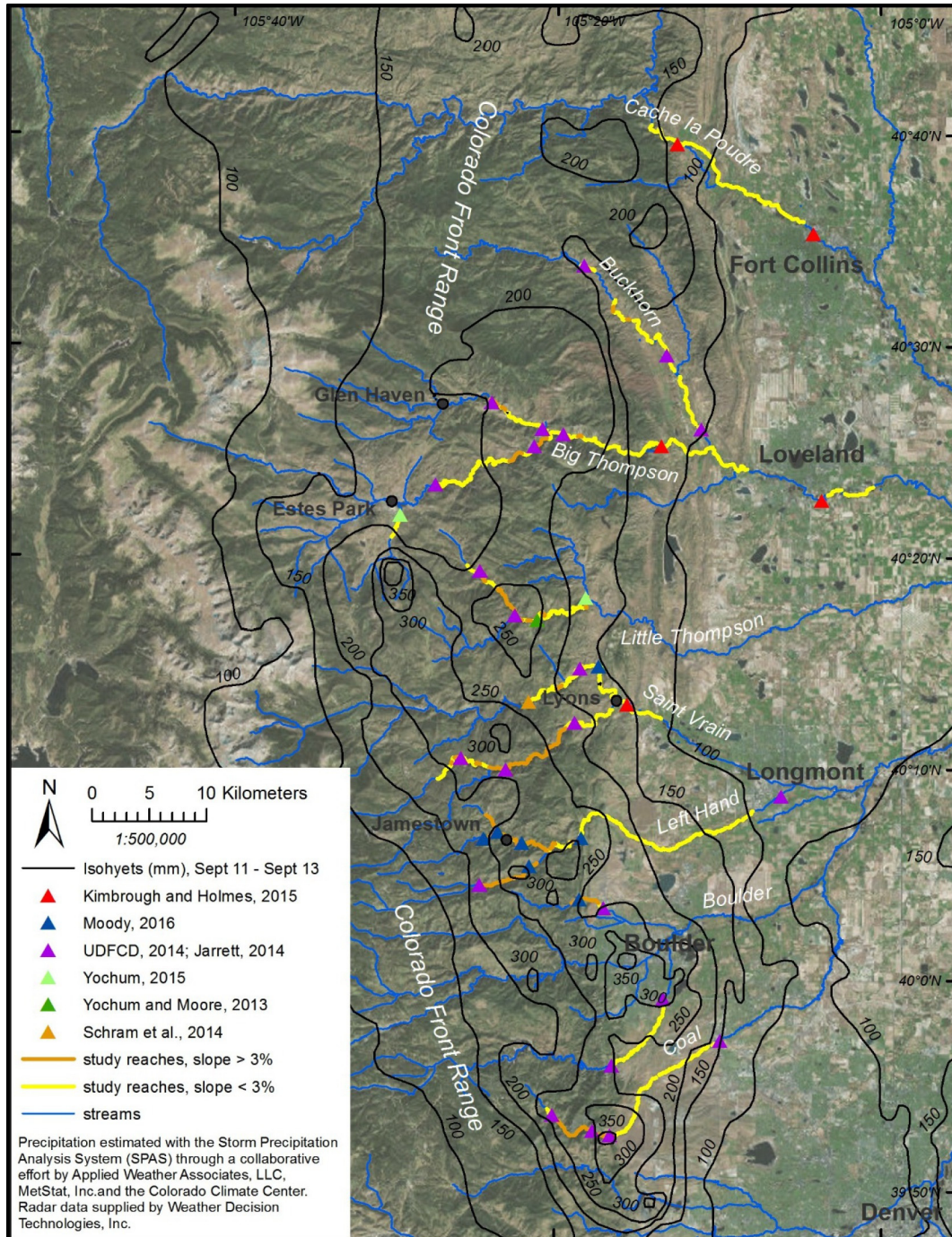


**Fig. 1.** Northern Front Range streams and communities most impacted by the 2013 Colorado Front Range flood, with study reaches, general channels slopes, and utilized peak flow estimate locations (by source). Isohyets (mm) of estimated rainfall depths for the most intense period of rainfall, from 0700 on 11 September to 0700 on 13 September, are also illustrated.

## 2. Background

Floodplain mapping based on flood-frequency relationships and hydraulic modeling of inundation extent and elevation is the standard method for characterizing flood hazards and informing floodplain management (e.g., Federal Emergency Management Agency, FEMA, floodplain planning and mapping). However, the area within stream corridors subject to flood hazards caused by geomorphic change typically is not considered. Flood hazard maps based on inundation alone can underestimate compounding threats and subjugate ecological function and services of stream corridors, suggesting the need for more comprehensive and sustainable approaches (Piegay et al., 2005; Biron et al., 2014; Olson et al., 2014). Fluvial hazard zone mapping techniques, which delineate areas at greater risk of geomorphic change within a stream corridor, have been available for some time (Graf, 1984), although the approach has been minimally adopted by regulatory agencies (Jagt et al., 2016) and is hindered by limited availability of quantitative tools for providing robust assessments (ASFP, 2016). Scientific tools and guidance are needed to predict locations and likelihoods of catastrophic geomorphic change at local (<10 channel widths), reach (~10 to 50 channel widths), and segment scales (up to ~5 km; Bizzi and Lerner, 2013).

Hydraulic thresholds of flood-induced geomorphic change have been previously related to total and unit stream power (Bull, 1979; Baker and Costa, 1987; Magilligan, 1992; Costa and O'Connor, 1995; Buraas et al., 2014; Magilligan et al., 2015). Bull (1979) focused on geomorphic thresholds and the role of stream power as it relates to streams in the context of anthropogenic change and other perturbations where streams are not in an equilibrium condition. Baker and Costa (1987) discussed the usefulness of  $\omega$  and channel boundary shear stress in assessing the role of floods in producing large geomorphic responses in fluvial systems and noted that the geomorphic effectiveness of floods was not consistently linked to the magnitude and frequency of an event. Magilligan (1992) emphasized that flood frequency and geomorphic instability are not especially relatable and estimated a minimum  $\omega$  and shear stress thresholds of 300 W/m<sup>2</sup> and 100 N/m<sup>2</sup>, respectively, for 'major morphological adjustments' in alluvial channels. These hydraulic thresholds were associated with events ranging from <2 times to >15 times the 100-year discharge due to the variability in local slopes and constraints by valley forms (floodplain width) and boundary materials (bedrock vs. alluvium or colluvium) within the study area. Buraas et al. (2014) also noted a 300 W/m<sup>2</sup> threshold for channel widening in Vermont (USA) streams impacted by Tropical Storm Irene and developed a new stream power-related metric, the bend stress parameter, that incorporates the radius of curvature of a meander bed in explaining the extent of widening.

The influence of flood duration on geomorphic change was emphasized by Costa and O'Connor (1995), who showed substantial variability in geomorphic change for a range of peak  $\omega$  and a more apparent pattern of increasing geomorphic response with an increase in energy expended per unit area over the flood duration. They hypothesized that an optimal combination of peak  $\omega$ , duration, and cumulative energy expenditure is required for the most geomorphically effective floods.

Total and unit stream power have been more generally associated with geomorphic change, including the utility of spatially relating erosion and deposition processes (Hooke and Mant, 2000; Kale, 2003; Fuller, 2008; Ortega and Heydt, 2009; Ferencevic and Ashmore, 2012; Bizzi and Lerner, 2013; Thompson and Croke, 2013; Gartner et al., 2015; Lea and Legleiter, 2015; Parker et al., 2015), and understanding geomorphic change induced from dam failures (Brooks and Lawrence, 1999) and glacial outburst floods, such as the cataclysmic Missoula floods (Benito, 1997) and floods in the Mount Everest region of Nepal (Cenderelli and Wohl, 2003). Additionally,  $\omega$  (in combination with a confinement index, percentage of reach length with artificial structures, and sediment supply area) has been utilized to predict channel width increases (Surian et al., 2016), though with rather low explained

variance. In general, the fundamental influence of stream power upon the potential for geomorphic change as well as the simplicity of its estimation using remotely sensed data have made this approach attractive to a number of researchers.

The inadequacy of  $\omega$  as the sole predictor of geomorphic change has, however, been noted in several studies. During a 1985 flood event in the central Appalachians, USA, substantial geomorphic alteration of channels and floodplain surfaces occurred at locations where  $\omega$  generally exceeded 300 W/m<sup>2</sup> (Miller, 1990); however,  $\omega$  was not a reliable predictor of geomorphic change for individual sites. In some cases, sites with nominal geomorphic change experienced  $\omega$  in excess of 1000 W/m<sup>2</sup> and other sites with severe erosion experienced  $\omega$  as low as 45 W/m<sup>2</sup>. Short-duration flooding induced by small dam failures with relatively high peak  $\omega$  resulted in small amounts of geomorphic impact (Costa and O'Connor, 1995). Likewise, the 2004 failure of a moderate-sized dam in Mississippi (USA) released a substantial peak flow of 4160 m<sup>3</sup>/s, with a flood duration of about 2 h (Yochum et al., 2008). Substantial geomorphic change was observed in the most upstream reach where average channel  $\omega$  of 1600 W/m<sup>2</sup> was experienced; however, minimal geomorphic change was observed within a well-vegetated reach downstream that experienced  $\omega$  of 800 W/m<sup>2</sup>. Peaks in  $\omega$  were not helpful for predicting overbank scouring along the Kamp River (Austria) during a flood in 2002 (Hauer and Habersack, 2009). Likewise, during the flooding induced from Tropical Storm Irene, a 300 W/m<sup>2</sup> minimum threshold was exceeded for 99% of a 60-km study reach of the Saxons River, but substantial channel widening occurred for only a small fraction of this length (Buraas et al., 2014). Notably, short-duration, high-energy floods can induce substantial sedimentological effects and can be considered geomorphically effective but have limited capability for channel widening in this humid setting (Magilligan et al., 2015). Additionally, using data from floods that occurred in Italy, in higher-gradient headwater streams, hydraulic variables alone were not good predictors of geomorphic change (Surian et al., 2016). The case may be that the initiation of major geomorphic change is tied to such a minimum threshold of 300 W/m<sup>2</sup>, but that exceedance of this threshold is far from certain to induce geomorphic instability due to variation in flood duration, geomorphic setting, planform, and resisting forces as affected by boundary materials, vegetation, and other factors.

More recent work on relating  $\omega$  to channel response has considered longitudinal variations in  $\omega$  as a predictor. For example, stream power averaged over 3 to 5 km upstream influences whether a reach's geomorphic response to flooding is degradational or aggradational (Bizzi and Lerner, 2013). Longitudinal decreases in stream power (negative stream power gradient) can be associated with depositional responses to floods, with increases in stream power associated with degradational responses (Gartner et al., 2015).

Relationships between stream power or stream power gradient and channel response to floods tend to be stronger over longer distances (Krapesch et al., 2011; Bizzi and Lerner, 2013; Gartner et al., 2015). Lea and Legleiter (2015) found only weak relationships between stream power gradient and sediment flux estimated using a combination of aerial photography analysis and field measurements in a study utilizing a relatively small spatial unit of analysis (60 m) on a single stream. Others have considered the influence of channel confinement by valley walls, finding that it tends to limit response but that it plays a role in a complex set of responses to drivers and resistors of geomorphic change (Nardi and Rinaldi, 2015; Surian et al., 2016).

## 3. Methods

### 3.1. Study area

During this flood, large portions of the Colorado Front Range foothills (Fig. 1) received heavy rainfall, with up to 460 mm falling in 10 days. The majority of the precipitation in and along the Front Range fell during 36 h on 11–12 September 2013. Rain gauge data from the most

severely affected areas of the foothills indicate that up to 380 mm fell in Larimer County, 460 mm fell in Boulder County, and 410 mm fell in El Paso County (CoCoRaHS, 2013; Gochis et al., 2015), the three counties most impacted by flooding. These rainfall depths are similar to the average annual precipitation in this semiarid landscape. The most substantial rainfall occurred on the edge of the high plains near the city of Boulder through the mid-elevation areas in Larimer and Boulder counties, between the elevations of 1700 and 3300 m (Fig. 1). This rain event established a new Colorado daily rainfall maximum of 316 mm (measured at Fort Carson, near Colorado Springs; Gochis et al., 2015).

As a result of these extreme rainfall depths and intensities, large floods occurred in the South Platte and Arkansas river basins in mountain valleys and canyons as well as on wide high plains valleys within a portion of Colorado's largest population center. Streams throughout the flooded areas were destabilized in many locations, leading to infrastructure, homes, and businesses being damaged or destroyed, an estimated \$2.9B in damages, and 9 human deaths (Aguilar, 2014). A combination of large discharges, steep channel slopes, and large quantities of sediment input from hillslope and bank failures, as well as debris flows, resulted in substantial geomorphic adjustments of the valley bottoms of the flood-affected streams (Fig. 2).

The geographic scope of this study is focused on streams of the northern Colorado Front Range within the South Platte River basin. From north to south, streams within the following watersheds were assessed: the Cache la Poudre River, Big Thompson River, Little Thompson River, Saint Vrain Creek, Left Hand Creek, Boulder Creek, and Coal Creek. Characteristics of the individual streams included in this study are provided in Table 1. These streams and reaches were selected based on data availability, visibility in aerial imagery, and variability in flood severity. Watershed areas contributing to the reaches included in the analyses ranged from 4.3 to 2900 km<sup>2</sup>. For additional information regarding the meteorologic, hydrologic, and geomorphic aspects of this event, refer to NWS (2013), Yochum and Moore (2013), Coe et al. (2014), Anderson et al. (2015), Gochis et al. (2015), Kimbrough and Holmes (2015), Tye and Cooley (2015), Yochum (2015), Moody (2016), and Rathburn et al. (2017).

Return periods of peak discharges within the study area ranged from moderate (25- to 50-year) to extreme ( $\geq 100$ -year; Yochum, 2015). The peak flow on Saint Vrain Creek in Lyons was especially remarkable as the estimated peak discharge value of 700 m<sup>3</sup>/s was more than twice the former maximum peak discharge for this gage with 122 years of record. Unit discharges were large for portions of this semiarid area, especially for the smallest watersheds. Unit discharges of up to 15 m<sup>3</sup>/s/km<sup>2</sup>

were observed for watersheds  $< 10$  km<sup>2</sup>, 5.2 m<sup>3</sup>/s/km<sup>2</sup> for watersheds ranging from 10 to 500 km<sup>2</sup>, and 1.2 m<sup>3</sup>/s/km<sup>2</sup> for watersheds  $> 500$  km<sup>2</sup> (Yochum, 2015).

### 3.2. Peak flow estimates

Peak flow estimates used in this study were obtained from a number of sources, including the U.S. Geological Survey (USGS; Kimbrough and Holmes, 2015; Moody, 2016), the Natural Resources Conservation Service (Yochum and Moore, 2013; Yochum, 2015), from the work of retired USGS research hydrologist Robert Jarrett (UDFCD, 2014; Jarrett, 2014), and from Schram et al. (2014). Peak flow estimates were developed using several methods. Lower flood peaks at stream gages were estimated using standard stream gage rating curves. Many streamflow gages were destroyed by the flood, and the majority of peak flow estimates were not made near existing stream gages. These estimates relied on either slope-area, culvert computation, contracted opening, conveyance, step-backwater, or critical depth methods (Kimbrough and Holmes, 2015; Yochum, 2015; Moody, 2016). Two-dimensional computational modeling was also performed for the peak flow estimate for the mainstem of Saint Vrain Creek (Kimbrough and Holmes, 2015). General methods for implementing these approaches to peak flow estimation are provided in Matthai (1967), Bodhaine (1968), and Dalrymple and Benson (1968), as well as in Hulsing (1967), Jarrett and Tomlinson (2000), Jarrett and England (2002), and Webb and Jarrett (2002) for the critical depth method.

Peak discharge values were assigned to reaches adjacent to the estimate and between significant tributaries. Where more than one peak discharge estimate existed along a length of stream without major intervening tributaries, the peak discharge was linearly interpolated between point estimates. In some cases, multiple flood peak estimates were made by different agencies within close proximity to one another. Here, we either used the peak estimate that resulted from a multiple method ensemble average (Moody, 2016) or the peak estimate that best aligned with discharge continuity between upstream and downstream peak values.

### 3.3. Aerial photography and LiDAR elevation data

Aerial photographs documenting pre- and post-flood conditions were obtained from a number of sources: U.S. Department of Agriculture, National Agriculture Imagery Program (NAIP, 100-cm resolution); World Imagery, ArcGIS Online (60 cm); WorldView-2, DigitalGlobe (46 cm); Google Earth (historical and post-flood imagery, various



Fig. 2. Post-flood geomorphic condition of a reach of North Saint Vrain Creek, near Lyons (9 April 2014). Flow direction is away from viewer.

**Table 1**  
Reach characteristics of streams included in analysis<sup>a</sup>.

| Stream             | Overall length (km) | Number of reaches | Average annual precipitation (mm) | Contributing area (km <sup>2</sup> ) | Stream slope (percent) | Flood return interval (years) | Unit stream power (W/m <sup>2</sup> ) | Geomorphic change classes |
|--------------------|---------------------|-------------------|-----------------------------------|--------------------------------------|------------------------|-------------------------------|---------------------------------------|---------------------------|
| Cache la Poudre    | 19.4                | 41                | 380 to 430                        | 2700 to 2900                         | 0.2 to 1.0             | 25 to 50                      | 80 to 700                             | 1 to 3                    |
| Fish Big           | 2.5                 | 6                 | 430                               | 34 to 41                             | 1.1 to 2.2             | >200                          | 310 to 730                            | 5                         |
| Thompson           | 44.0                | 93                | 380 to 460                        | 430 to 1500                          | 0.2 to 6.3             | 100                           | 28 to 4900                            | 2 to 6                    |
| N.F. Big Thompson  | 6.9                 | 14                | 430                               | 190 to 220                           | 1.4 to 3.6             | >100                          | 180 to 2900                           | 5                         |
| Buckhorn           | 18.7                | 46                | 410 to 480                        | 130 to 370                           | 0.7 to 5.0             | 25 to 50                      | 300 to 4700                           | 3 to 6                    |
| Little Thompson    | 19.6                | 45                | 460 to 480                        | 24 to 130                            | 1.3 to 10.5            | –                             | 210 to 7000                           | 2 to 6                    |
| N. Saint Vrain     | 15.0                | 39                | 410 to 460                        | 260 to 320                           | 0.5 to 6.4             | –                             | 310 to 7000                           | 4 to 6                    |
| Middle Saint Vrain | 7.1                 | 21                | 510 to 530                        | 70 to 83                             | 2.0 to 8.9             | –                             | 180 to 3700                           | 2 to 5                    |
| S. Saint Vrain     | 15.2                | 31                | 410 to 510                        | 170 to 240                           | 1.0 to 7.0             | –                             | 360 to 3800                           | 4 to 5                    |
| Saint Vrain        | 4.4                 | 11                | 380 to 410                        | 560 to 570                           | 0.8 to 1.0             | >200                          | 85 to 600                             | 3 to 5                    |
| Left Hand          | 31.8                | 84                | 360 to 530                        | 46 to 180                            | 0.3 to 6.4             | >200                          | 60 to 4700                            | 2 to 5                    |
| James              | 6.6                 | 18                | 510 to 530                        | 23 to 48                             | 2.8 to 5.8             | –                             | 690 to 2900                           | 3 to 5                    |
| Little James       | 2.2                 | 7                 | 510 to 530                        | 4.3 to 7.9                           | 5.0 to 8.0             | –                             | 1000 to 2400                          | 3 to 6                    |
| Fourmile Canyon    | 3.4                 | 8                 | 480 to 530                        | 12 to 19                             | 2.6 to 5.1             | –                             | 120 to 3100                           | 5                         |
| S. Boulder         | 8.2                 | 17                | 460 to 510                        | 290 to 330                           | 0.8 to 2.0             | 50                            | 130 to 640                            | 2 to 3                    |
| Coal               | 21.1                | 50                | 430 to 560                        | 23 to 69                             | 1.0 to 6.1             | 100 to 200                    | 440 to 4700                           | 2 to 5                    |

<sup>a</sup> The range of average annual precipitation (Daly et al., 2008) is for the assessed reaches of each stream. Flood recurrence intervals are based on a log-Pearson III analysis of stream gage records (including the 2013 peak flow estimates), using Bulletin 17B methods (IACWD, 1982).

resolutions); Colorado Water Conservation Board (30 cm); and from the Colorado Department of Transportation (along US-36 and US-34, 10 cm).

Post-flood aerial light detection and ranging (LiDAR) data were collected over the study area by a USGS and FEMA collaboration on 16 October 2013. Additionally, pre-flood LiDAR data were collected by Boulder County on 25 October 2011. LiDAR data were classified and had point densities ranging from 5 to 10 points/m<sup>2</sup>. Bare earth digital elevations models (DEMs) with 0.75 × 0.75 m grid cells were generated from these data by the respective agencies and accessed via an online database ([www.geodata.co.gov](http://www.geodata.co.gov)). Pre-flood LiDAR data were available for streams within Boulder County and for a limited number of streams in Larimer County.

The DEMs were used in a number of ways in this study. Channel and valley cross section geometry was extracted for use in hydraulic modeling to estimate in-channel  $\omega$  as described below. Hillshade rasters were generated to aid in estimating channel top widths and in characterizing channel change in conjunction with aerial imagery. Finally, in areas where pre- and post-flood LiDAR coverage was available, DEMs of difference (DoD) were developed to visualize geomorphic change and to aid in classification (Wheaton et al., 2010). These DoDs were created by calculating the elevation difference between pre- and post-flood rasters with aligned and equal-sized grid cell sizes. Rigorous methods exist to quantify uncertainty in DoDs, especially if the uncertainty of the original DEMs can be quantified (Lane et al., 2003; Wheaton et al., 2010). We did not have access to the original LiDAR data used to generate the DEMs, and we are using the DoDs in a qualitative, visual manner to aid in channel response classification. Therefore, we used an arbitrary value of ±0.25 m in elevation difference to threshold our DoDs and remove this assumed noise from our visual assessment of geomorphic change. This threshold value approximates the outer bound of uncertainty values found in other DoDs of fluvial systems (Lane et al., 2003; Wheaton et al., 2010).

### 3.4. Channel confinement

Channel confinement, defined as the ratio of the valley width to the top-of-bank channel, was evaluated as a predictor variable for geomorphic change. This metric quantifies the relative space in which a channel

can adjust laterally in response to floods (Wohl, 2010). Confinement was extracted from a valley classification geospatial data product covering the majority of the reaches in this study area following the methods outlined in Carlson (2009) and Wohl (2010). Channel confinement ratios are derived from valley widths delineated from a 10 × 10 m DEM and a regional downstream hydraulic geometry relation for channel top width. Elsewhere, confinement was calculated from floodplain widths estimated from valley cross sections extracted from the LiDAR-based DEMs and channel top widths estimated using a combination of LiDAR-based hillshade rasters and aerial imagery. Pre-flood channel widths derived from these data are used to calculate the confinement ratio.

### 3.5. Stream power estimates

Total stream power is computed as

$$\Omega = \gamma Q S_f \quad (1)$$

where  $\Omega$  is total stream power (W/m),  $\gamma$  is the specific weight of water (N/m<sup>3</sup>),  $Q$  is the discharge (m<sup>3</sup>/s), and  $S_f$  is the friction slope of the flow within a given reach (estimated as the bed slope for much of the study). Unit stream power normalizes  $\Omega$  by the peak flow width ( $w$ ) and is computed as

$$\omega = \frac{\Omega}{w} = \frac{\gamma Q S_f}{w} \quad (2)$$

In confined reaches within the foothills of the study area, total peak discharge, flow width, and reach-averaged slope were used to estimate peak  $\omega$  ( $n = 248$ ). Computation of  $\omega$  in reaches with wide floodplains can lead to underestimating the magnitude of in-channel  $\omega$  as Miller (1990) experienced when using  $\omega$  normalized with the floodplain or valley width. Because erosive energy from a flood is concentrated in the channel, normalizing  $\Omega$  by the floodplain width underestimates the value of  $\omega$  experienced by the channel where geomorphic change dominates. Hence, in stream reaches with substantial floodplains, one-dimensional standard-step hydraulic modeling (HEC-RAS, version 5.0) was performed to differentiate in-channel and floodplain discharge for

calculating peak  $\omega$  ( $n = 283$ ). The HEC-RAS modeling also estimates the energy grade line slope, which, along with the channel width, was used to calculate  $\omega$  for these reaches. This modeling was performed using post-flood channel geometry extracted from the post-flood LiDAR-generated DEMs. We also consider change in  $\omega$  and unit stream power gradient ( $d\omega/dx$ ) at the reach scale as a predictor of channel response.

### 3.6. Reach delineation and geomorphic change classification

The fundamental unit of assessment for this study is the stream reach, which was delineated along the centerline of the post-flood channel. Reaches were delineated along relatively homogenous stretches of channel response to the flood and geomorphic setting, defined by channel confinement, slope, and boundary resistance. Each reach is assigned its own values of predictor variables (e.g.,  $\omega$ , channel confinement) and a geomorphic change classification (response variable). Stream reaches vary in length but do not exceed 500 m. This upper limit reflects typical variability in valley and channel form and observed variability in geomorphic adjustments during the flooding.

A qualitative classification scheme was developed to describe geomorphic change of each stream reach. The scheme was developed using remotely-sensed and field-based observations of the variety of

geomorphic adjustments that were caused by this flood. The two most disturbed classes (5 and 4) are illustrated using side-by-side pre- and post-flood imagery (Fig. 3). We used the following definitions for each class:

1. No detected geomorphic change.
2. Infrequent eroded streambanks (<25% of overall streambank length).
3. Numerous eroded streambanks (>25% of overall streambank length).
4. Substantially widened channel over the majority of the reach length.
5. Major geomorphic change, with avulsions, braiding, or roadway embankments and high terraces eliminated or substantially eroded by erosional and/or depositional processes.
6. Narrow valley form (canyon) limits geomorphic adjustment potential, with no substantial pre-flood floodplains detected.

Geomorphic change classes were assigned primarily using remotely sensed data, specifically pre- and post-flood high resolution aerial imagery and LiDAR-derived visualizations. If the remotely sensed data were insufficient to determine the geomorphic change class, which was generally caused by excessive tree cover, field visits to the stream reaches were performed. Reaches were excluded from the analysis if adequate



**Fig. 3.** Examples of geomorphic change for classes 5 and 4, with paired pre- and post-flood imagery. The upper pair illustrates class 5 geomorphic change, with channel adjustment and the resulting elimination of the armored US-34 roadway embankment along the Big Thompson River. The lower pair, also for the Big Thompson River, illustrates class 4 geomorphic change with the channel substantially widening for a majority of the reach length but not shifting or avulsing. Sediment deposition on the floodplain surface is also apparent, but woody riparian vegetation was not substantially impacted otherwise. Imagery sources: ArcGIS Online and DigitalGlobe. (Note: dates are month/day/year.)

data were not available to evaluate immediate post-flood channel response and where anthropogenic manipulation of the stream channels and floodplain were too substantial to make a reasonable field determination of the response class.

Considering the subjective nature of this geomorphic change classification approach, a blind quality assurance process was utilized to reduce variability. Stream reaches were delineated (by one of the authors) and the geomorphic change class assigned to each reach. Then the classification and stream power attributes were stripped from the database and shared with one of the other authors for their independent assessment of geomorphic change. The two independent assessments of geomorphic change were then compared and a consensus was arrived at for each reach.

### 3.7. Statistical analyses

The categorical geomorphic change data were tested for significant differences in median values using non parametric Analysis of Variance (ANOVA) procedures, specifically the Kruskal-Wallis one-way analysis of variance on rank (Kruskal and Wallis, 1952). This non parametric procedure was used due to data non-normality, as tested using the Kolmogorov-Smirnov procedure. The test statistic for Kruskal-Wallis is denoted as  $H$ . Pairwise multiple comparisons of the classifications were performed using Dunn's method (Dunn, 1961). The ANOVA testing was performed in SigmaPlot (version 13.0). Unit stream power cumulative frequencies were computed using a Cunnane (1978) distribution.

To test whether  $\omega$  values were significantly correlated with the ordinal geomorphic categorical data, the Kendall rank correlation ( $\tau$ -b) was calculated and tested for significance using the Kendall package (McLeod, 2015) in R (version 3.2.2; R Core Team, 2015).

We explored whether remotely sensed and stream-power-related variables could predict the ordinal geomorphic change classifications assigned to each reach using a cumulative logit model. For a given set of predictor variables associated with a stream reach (e.g.,  $\omega$  and channel confinement), this model estimates the probability that the geomorphic change of a particular reach will fall into each response class. The response class with the highest probability is the predicted geomorphic response outcome. We only included classes 2 to 5 as only four class 1 responses were observed in our data set.

This model is a special case of the generalized linear model in which the response variable is ordinal and is fitted using a maximum likelihood approach. The cumulative logit model predicting the ordinal geomorphic response variable  $Y$  for each observation ( $i$ ) from predictor variables ( $X$ ) has the form

$$\text{logit}(P(Y_i \leq j)) = \log \left[ \frac{P(Y_i \leq j)}{1 - P(Y_i \leq j)} \right] = \theta_j - \beta_1(X_{1,i}) - \beta_2(X_{2,i}) - \dots \quad (3)$$

with  $i = 1, \dots, n$  observations and  $j = 1, \dots, J - 1$  thresholds between response classes. The parameter  $\theta_j$  represents the  $J - 1$  cumulative logit threshold values demarking the transition from response class 2:3, ..., 5:6. The  $\theta_j$ 's can be thought of as model intercept values in logit space. They represent the log odds of falling into a particular category when all predictor variables are equal to zero. The  $\beta$ 's are predictor variable coefficients that remain constant across all  $\theta_j$ 's, meaning that there is not a different relationship between predictor and response variables between geomorphic change classes. This is known as the proportional odds assumption for cumulative logit models. To test that a given model meets this assumption, a likelihood ratio test between models with fixed  $\beta$ 's and unfixed  $\beta$ 's that are allowed to vary with  $j$  was conducted as outlined in Christensen (2015a).

We used the `clm()` function in the ordinal package (Christensen, 2015b) in R (version 3.2.2; R Core Team, 2015) to create and fit the cumulative logit models. Numerous predictor variables were explored in this modeling framework including  $\omega$ ,  $\Omega$ , channel slope, the gradient

and difference of  $\omega$  and  $\Omega$  between adjacent up- and downstream reaches, channel confinement ratio, and a binary channel confinement categorical variable (Table 2). Channels were considered confined for the binary confinement metric if the confinement ratio was  $\leq 7$  following Carlson (2009). A sensitivity analysis on confinement ratio threshold values (from 5 to 10) did not improve model performance over the chosen value of 7. Total and unit stream power gradient,  $d\Omega/dx$  and  $d\omega/dx$ , were calculated as the difference in unit (total) stream power between down- and upstream reaches divided by the total length of the two reaches. In addition to different combinations of predictor variables, we also considered different subsets of the data collected including all reaches, all reaches with slopes  $< 3\%$ , all reaches with response classes 4 and 5 as well as classes 2 and 3 combined, and finally a data set with the lumped response classes and reaches with slopes  $< 3\%$ .

The performance of models and model parameters were evaluated based on the significance of the parameter coefficients, and the model accuracy or the percent of correctly predicted geomorphic change classes based on a 'leave-one-out' cross-validation approach. This method uses a model to predict the change class of a reach that has been left out of the fitting; this is repeated over all reaches. This approach maintains model independence of each observation used to assess its accuracy. The significance of the predictor variables was evaluated using a likelihood ratio test with the  $\chi^2$  distribution.

## 4. Results

A total of 531 reaches were assessed on 226 km of streams impacted to various extent by the 2013 flood event in the Cache la Poudre River, Big Thompson River, Little Thompson River, Saint Vrain Creek, Left Hand Creek, Boulder Creek, and Coal Creek watersheds, which are all located in the South Platte River basin in and adjacent to the Colorado Front Range foothills. Reach lengths varied from 71 to 500 m, with an average of 426 m. A variety of stream channel scales and types were included in the analysis: watershed areas contributing to the stream reaches ranged from 4.3 to 2900 km<sup>2</sup>; and stream channel slopes varied from 0.2 to 10.5%. A summary of reach and reach response information grouped by watershed is provided (Table 1).

### 4.1. Geomorphic change summary

Longitudinal plots of  $\omega$  evaluated on a reach scale show distinct patterns (Fig. 4). In streams that flow from the foothills onto the high plains within the study area (e.g., Coal Creek, Left Hand Creek, St. Vrain Creek, Big Thompson River, and Poudre River), a progressive decrease in  $\omega$  is observed as higher gradient, confined reaches transition to lower gradient and less confined reaches. Nevertheless, the geomorphic change frequently remained high along the downstream portions of these streams.

Unit stream power has a positive and significant monotonic relationship with the geomorphic change classification, based on the Kendall rank coefficient of 0.83 ( $P < 0.001$ ). Data with geomorphic change

**Table 2**  
Cumulative logit model predictor variables.

| Variable  | Definition                                  |
|---|---|
| $\Omega$ , $\omega$                                 | Stream power, unit stream power             |
| $\Delta\Omega/\Delta x$ , $\Delta\omega/\Delta x^a$ | Stream power and unit stream power gradient |
| $\Delta\Omega$ , $\Delta\omega^b$                   | Unit stream power difference                |
| $S$   | Average channel slope                       |
| $conf^c$  | Channel confinement ratio                   |
| $conf.cat^d$  | Channel confinement category                |

<sup>a</sup> Defined as the difference between downstream and upstream stream power for adjacent reaches divided by their combined lengths.

<sup>b</sup> Difference between downstream and upstream stream power.

<sup>c</sup> Valley width divided by channel top width.

<sup>d</sup> Confined category defined as confinement ratio  $< 7$ .

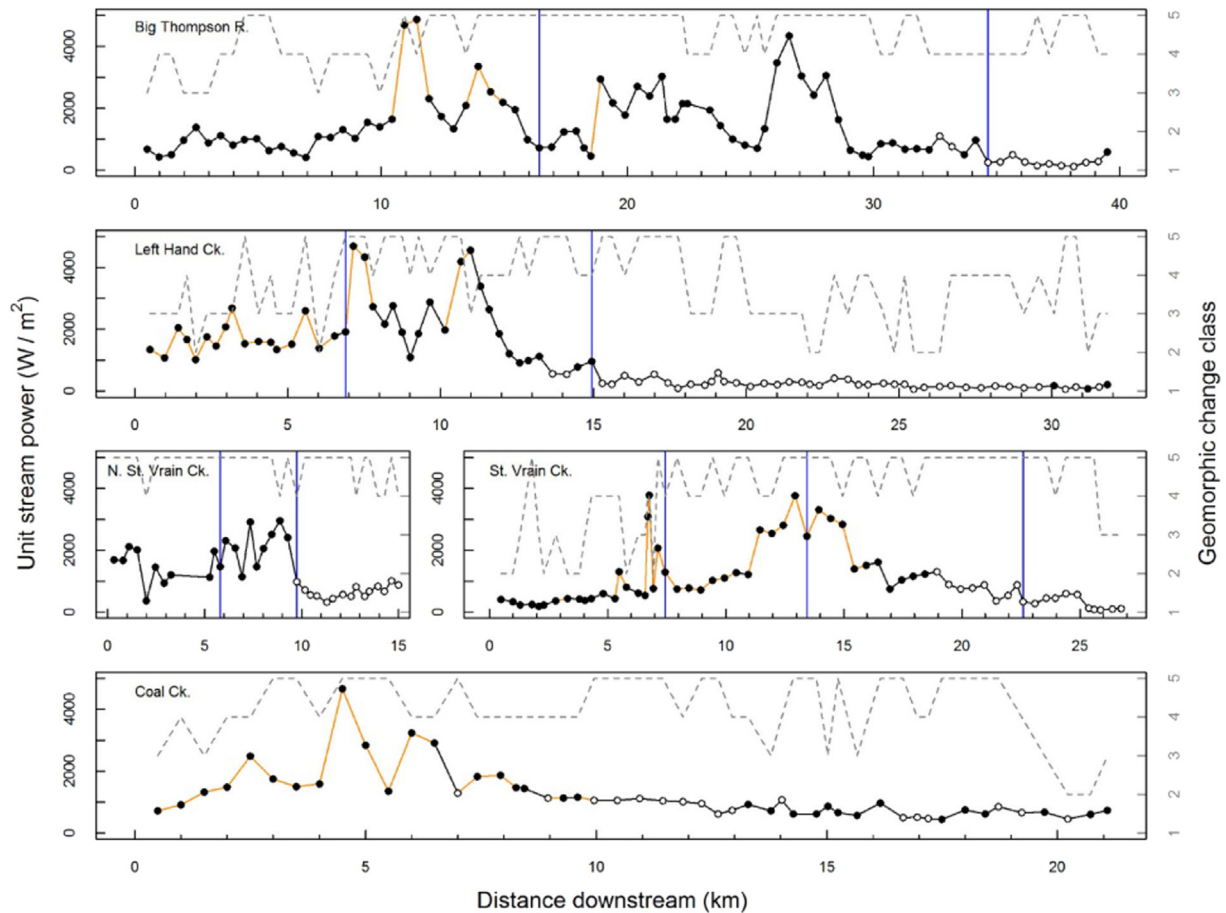


**Fig. 4.** Longitudinal unit stream power ( $\omega$ ) for selected streams (black solid line, left hand y-axis) with associated geomorphic change class (grey dashed line, right hand y-axis). Orange segments represent reaches with slopes  $\geq 3\%$ . Closed circles represent confined reaches and open circles unconfined. Blue vertical lines represent confluences with significant tributaries. The North Fork of the Big Thompson joins the Big Thompson at 16.5 km; James Creek joins Left Hand Creek at 7 km; St. Vrain Creek represents continuous data from Middle St. Vrain Creek to its confluence with South St. Vrain Creek (7.5 km) then to St. Vrain Creek at its confluence with North St. Vrain Creek at 22.5 km.

classes of 2 through 6 are illustrated in box plots (Fig. 5A). Reaches with a geomorphic change class of 1 (no detected geomorphic change,  $n = 4$ ,  $\omega = 240\text{--}460\text{ W/m}^2$ ) were excluded as they were not systematically sampled. Reaches with a geomorphic change class of 6 (narrow valley form limits geomorphic adjustment potential) were excluded from additional analyses as they inherently have little potential for adjustment. Median  $\omega$  increased from 280 to 370  $\text{W/m}^2$  for stream channels with infrequent eroded banks (2) to numerous eroded banks (3), and 970 to 1100  $\text{W/m}^2$  for channels with substantially widened channels (4) to major geomorphic change (5). Unit stream power at the 10th percentile for both of the substantial geomorphic change classes (4, 5) was approximately 300  $\text{W/m}^2$  (280 and 300  $\text{W/m}^2$ , respectively), a previously estimated threshold above which ‘catastrophic’ change occurs (Magilligan, 1992). However,  $\omega$  values at the 90th percentile for classes with less geomorphic change (2 and 3) were 700 and 1500  $\text{W/m}^2$ . An ANOVA using the Kruskal–Wallis test with three degrees of freedom [ $H(3) = 114.3, P < 0.001$ ] and Dunn’s pairwise tests for individual differences between these categorical geomorphic change descriptors indicate that the median  $\omega$  values for change classes 2 and 3 differ from 4 and 5 ( $P < 0.001$ ), the median values of 2 and 3 differ from each other, though less significantly ( $P = 0.039$ ), and 4 and 5 do not differ ( $P = 1.000$ ).

Outlier values present in Fig. 5A offer an opportunity for improved understanding of mechanisms underlying anomalous channel changes. Reaches that experienced higher peak flow  $\omega$  but the lower geomorphic change classes of 2 or 3 (upper outlying classes 2 and 3 points in Fig. 5A) typically had higher channel gradients and step pool or cascade bedforms that generally increase flow resistance. Additionally, a

number of reaches that experienced larger amounts of geomorphic change (classes 4 and 5) had relatively low  $\omega$  (lower outlying classes 4 and 5 points in Fig. 5A). In particular, class 5 reaches were often downstream of substantial reductions in  $\omega$  (downstream of canyon mouths, with reductions in slope and increased valley width), resulting in reduced sediment and debris transport capacity, channel and floodplain deposition, and channel braiding. The geomorphic changes in these braided reaches were dominated by depositional processes rather than erosional. Channel confinement also affects the relationship between degree of response and  $\omega$ . For a given classification of channel response, associated  $\omega$  values were smaller for unconfined reaches versus confined reaches (Fig. 6). Unconfined reaches (valley width:channel width  $> 7$ ) require less  $\omega$  for a given degree of geomorphic change and appear more geomorphically sensitive to floods.

To garner greater insight into relationships between  $\omega$  and geomorphic change, we stratified the data set based on physical mechanisms that may explain the outliers. Given that higher-gradient stream channels were often in geomorphic settings that impart resistance to channel change despite high stream power, the data set was divided between channels with slopes  $< 3\%$  ( $n = 358$ ) and slopes  $\geq 3\%$  ( $n = 117$ ). This division was set at an approximate point where step-pool and cascade mechanisms and flow dynamics begin to substantially increase flow resistance (Montgomery and Buffington, 1997; Yochum et al., 2014). In-field visual inspection of a sample of streams with slopes  $\geq 3\%$  indicated more pronounced bedforms induced primarily by boulder-sized clasts.

We further divided the data set based on the observation that geomorphic change class 5 is, in places, associated with large reductions

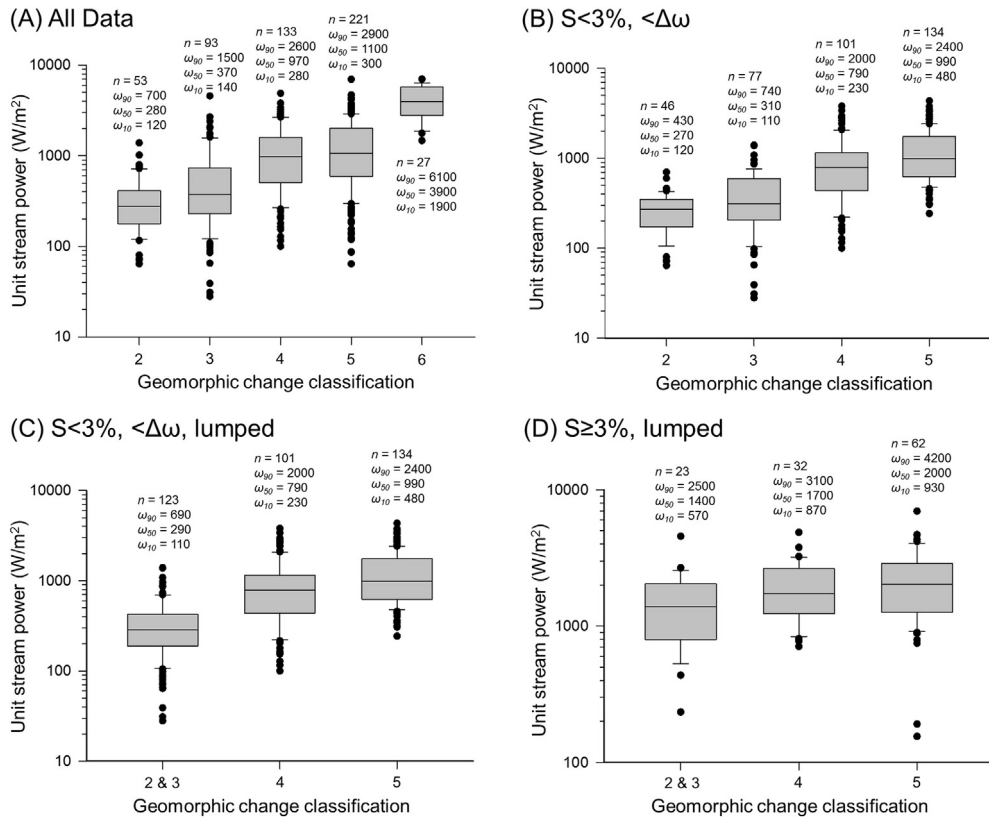


**Fig. 5.** Boxplots of unit stream power ( $\omega$ ) versus geomorphic change. Unit stream power is in  $\text{W/m}^2$ , with the subscript referring to the exceedance frequency within the data set, and  $n$  being the number of data points in each geomorphic classification. Geomorphic change class definitions: 2 – infrequent eroded streambanks (<25% of overall streambank length); 3 – numerous eroded streambanks (>25% of overall streambank length); 4 – substantially widened channel over the majority of the reach length; 5 – major geomorphic change, with avulsions, braiding, or roadway embankments and high terraces eliminated or substantially eroded by erosional and/or depositional processes. The number of data points as well as the median, 10th, and 90th percentiles are provided for each box plot. Part A provides all the collected data (sans class 1 reaches), part B includes only reaches with channel slopes < 3% and excludes class 5 reaches with large reductions in  $\omega$  induced by changes in valley confinement (< $\Delta\omega$ ), part C includes the same data as part B though with classes 2 & 3 combined, and part D includes only reaches  $\geq 3\%$  and classes 2 & 3 combined.

in  $\omega$  induced by changes in valley confinement that result in channel instabilities from decreased sediment and debris transport capacity. Specifically, we removed 25 reaches that experienced greater amounts of geomorphic change (class 5) as a result of large reductions in  $\omega$  (>50% reduction), deposition, and braiding across floodplains below canyon mouths. These reaches were in the Big Thompson, North Fork of the Big Thompson, Saint Vrain, Left Hand, and Fourmile Canyon.

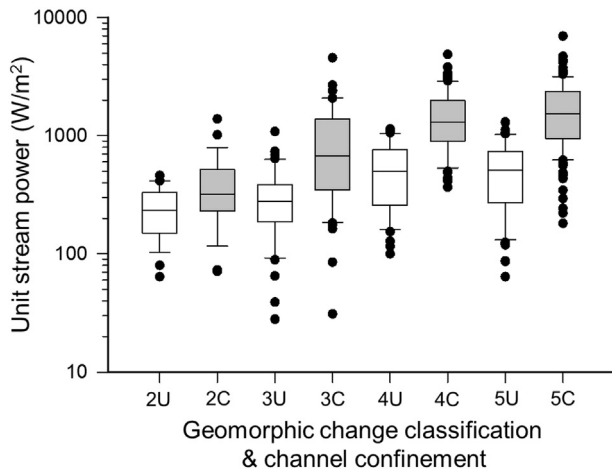


**Fig. 6.** Boxplots of unit stream power ( $\omega$ ) versus geomorphic change class and channel confinement class for the complete dataset. U: unconfined; C: confined.

For reaches with slopes < 3% and with noted class 5 reaches excluded ( $n = 358$ ), box plots for geomorphic change classes 2 through 5 illustrate more predictive capability between  $\omega$  and geomorphic change (Fig. 5B). Median power increases from 270 to 310  $\text{W/m}^2$  for stream channels with infrequent eroded banks (2) to numerous eroded banks (3), and 790 to 990  $\text{W/m}^2$  for channels with substantially widened channels (4) to major geomorphic change (5). The ANOVA testing of this subset of data indicates a statistically significant difference among change classes [ $H(3) = 148.3, P < 0.001$ ]. Dunn's pairwise testing indicates that change classes 2 and 3 differ from both 4 and 5 ( $P < 0.001$ ) and that 4 and 5 differ from each other ( $P = 0.017$ ), but that 2 and 3 do not significantly differ from each other ( $P = 0.322$ ).

This subset of data was subsequently combined into three classes: classes 2 and 3 were lumped (infrequent to numerous eroded streambanks), and classes 4 and 5 were kept separate. This was done for reaches with slopes of < 3% (Fig. 5C) and  $\geq 3\%$  (Fig. 5D). For reaches with slopes < 3%, the data indicate a positive association between  $\omega$  and geomorphic change, with the median power at 290  $\text{W/m}^2$  for reaches with infrequent to numerous eroded banks (2 and 3), and 790 and 990  $\text{W/m}^2$  for channels with substantially widened channels (4) and major geomorphic change (5), respectively. Unit stream power at the 10th percentile for substantially widened channels over the majority of their length (4) is 230  $\text{W/m}^2$  but higher at 480  $\text{W/m}^2$  for channels with major geomorphic change (5). The 90th percentile for classes with less geomorphic change (2 and 3) was 690  $\text{W/m}^2$ . ANOVA testing [ $H(2) = 144.6, P < 0.001$ ] indicates that change classes 2 and 3 differ from both 4 and 5 ( $P < 0.001$ ), and 4 and 5 significantly differ from each other in this subset of data ( $P = 0.008$ ). Subsampling the database for reaches with slopes < 3% and removing the unconfined reaches located below

confined river segments clarified relationships between  $\omega$  and geomorphic change classes. For stream reaches with slopes  $\geq 3\%$ ,  $\omega$  was higher than the lower gradient data, with median values increasing for lumped classes 2 and 3, 4, and 5 (Fig. 5D). ANOVA testing [ $H(2) = 6.0, P = 0.05$ ] indicated that 2 and 3 significantly differed from 5 ( $P = 0.043$ ), but other differences were not significant given the number of observations.

4.2. Cumulative logit modeling

Models fit to the entire data set with all five response classifications demonstrated convergence problems and poor prediction of geomorphic response classes (<50% accuracy, Table 3). This is likely due to the wide variability in  $\omega$  associated with each change class as well as the longitudinal and slope effects discussed in the previous section. Models fit to subsetted data with slopes < 3% and with geomorphic response classes 4 and 5 combined (four classes instead of five) performed well with correct classification accuracies ranging from 68% to 74%. Models based on just two classes (classes 2 and 3 lumped, classes 4 and 5 lumped) resulted in the greatest accuracy (72% to 83%).

In general, all models across all data sets tended to overpredict the number of classes 4 and 5 responses and underpredict responses for classes 2 and 3. Observed geomorphic change classes were skewed toward classes 4 and 5 in response to the extreme nature of this flood in much of the study area. This resulted in models with fitted parameters weighted to these greater response classes. Cumulative logit models perform best with a similar distribution of observations in each response class. A selection of fitted models and results are presented in Table 4.

Models with either  $\omega$  or  $\Omega$  as the sole predictor variable performed fairly well with 68% and 71%, respectively, of observed channel change classifications predicted correctly in the data set with <3% slopes and classes 4 and 5 lumped. Adding other predictor variables, such as channel confinement and unit (total) stream power gradient ( $\Delta\omega/\Delta x, \Delta\Omega/\Delta x$ ) or difference ( $\Delta\omega, \Delta\Omega$ ), improved model skill but only marginally.

**Table 3**  
Cumulative logit model accuracy results.

| Model | Predictor variables <sup>a</sup>               | Data set <sup>b</sup> | Model sensitivity by geomorphic change category (%) <sup>c</sup> |     |    |    |     | Model accuracy (%) <sup>d</sup> |    |
|-------|--|-----------------------|--|-----|----|----|-----|---------------------------------|----|
|       |  |                       | 2  | 2-3 | 3  | 4  | 4-5 |                                 |    |
| 1     | $\omega + \omega.conf$                         | 1                     | 4  |     | 19 | 10 |     | 85                              | 44 |
| 2     | $\Omega + \Omega.conf.cat$                     | 1                     | 0  |     | 29 | 33 |     | 78                              | 49 |
| 3     | $\omega + \omega.conf.cat$                     | 2                     | 0  |     | 50 | 9  |     | 75                              | 43 |
| 4     | $\Omega + \Omega.conf.cat$                     | 2                     | 2  |     | 58 | 32 |     | 75                              | 52 |
| 5     | $\Omega + \Omega.conf + \Delta\Omega$          | 3                     | 33   |     | 35 |    | 92  |                                 | 74 |
| 6     | $\omega + conf.cat + \Delta\omega$             | 3                     | 18   |     | 26 |    | 92  |                                 | 70 |
| 7     | $\Omega$                                       | 3                     | 15   |     | 32 |    | 93  |                                 | 71 |
| 8     | $\omega$                                       | 3                     | 7  |     | 21 |    | 93  |                                 | 68 |
| 9     | $\Omega + \Omega.conf + \Delta\Omega/\Delta x$ | 4                     |  | 71  |    |    |     | 86                              | 81 |
| 10    | $\omega + conf.cat + d\omega$                  | 4                     |  | 63  |    |    |     | 84                              | 77 |
| 11    | $\Omega$                                       | 4                     |  | 67  |    |    |     | 89                              | 82 |
| 12    | $\omega$                                       | 4                     |  | 63  |    |    |     | 85                              | 78 |
| 13    | $\Omega + \Omega.conf$                         | 5                     |  | 60  |    |    |     | 90                              | 81 |
| 14    | $\omega * conf + \Delta\omega$                 | 5                     |  | 47  |    |    |     | 91                              | 78 |
| 15    | $\Omega$                                       | 5                     |  | 60  |    |    |     | 92                              | 83 |
| 16    | $\omega$                                       | 5                     |  | 37  |    |    |     | 91                              | 75 |
| 17    | $S + conf$                                     | 5                     |  | 12  |    |    |     | 97                              | 72 |

<sup>a</sup> See Table 1 for predictor variable definitions. The operator (\*) denotes an additive and an interaction affect between the two variables. The operator (:) denotes an interaction effect between two variables.

<sup>b</sup> Data set 1 is the complete data set; data set 2 contains only reaches with slopes < 3%; data set 3 is the same as 2 but with geomorphic change categories 4 and 5 lumped into one response category; data set 4 is the same as 2 but with categories 2 and 3 lumped and categories 4 and 5 lumped (two response categories); and data set 5 is the complete dataset with the same two response categories as in data set 4.

<sup>c</sup> Model sensitivity is defined as the percent of correctly-predicted geomorphic responses within each response category based on a leave-one-out analysis.

<sup>d</sup> Model accuracy is the percent of geomorphic response category classes correctly predicted overall based on a leave-one-out analysis.

For example, by adding  $\Omega$  gradient and channel confinement to the  $\Omega$  predictor, percent predicted correctly increased from 71% to 74%. These gains in predictive performance were made in geomorphic change classes 2 and 3, and the additional variables were significant in the model as evaluated by likelihood ratio tests between models with and without parameters of interest (Table 4). Model 16, based on the entire data set with the two change categories (minor and major change) and only using  $\Omega$  as a predictor variable, had an accuracy of 84%. This is not surprising given the binary response to be predicted. It is interesting to note that additional predictor variables did not increase the accuracy of models based on two change classifications (lumped classes 2 and 3, and 4 and 5). Single predictor variable models were compared with the null model for variable significance testing. A model based on slope and channel confinement ratio performed reasonably well in the two response classification data set with an overall accuracy of 72%. However, this model grossly overpredicted responses for the lumped classes 4 and 5.

In general,  $\Omega$  tends to provide higher prediction accuracy in these models compared to  $\omega$ . Channel confinement ratio as a continuous variable tends to perform about as well as a simple binary variable where the confined class is defined as a confinement ratio  $\leq 7$  and unconfined as  $> 7$ . The categorical confinement variable was a significant predictor variable in most models; however, the continuous confinement variable was significant only in some cases. Models that included slope, a more readily evaluated predictor, in place of  $\Omega$  or  $\omega$  performed poorly, tending to predict only class 4 or 5 responses over nearly all reaches.

The best performing models include  $\Omega$  or  $\omega$ , the difference or gradient of unit (total) stream power, and one of the confinement variables as predictors (Tables 3 and 4). To interpret the model parameters, we consider  $\omega$ -based model 6 fitted to reaches with slopes < 3% and with response classes 4 and 5 combined. Based on the coefficients of this model (predictor variable coefficient values,  $\beta_i$ , Table 4), for a 100 W/m<sup>2</sup> increase in  $\omega$ , the odds ratio of moving up in geomorphic change class is 1.6 (60% higher) with the other variables constant. The probability of moving up a class for a 300 W/m<sup>2</sup> increase in stream power is 80%. For a 100 W/m<sup>2</sup> unit decrease in  $\omega$  from upstream to downstream reaches ( $\Delta\omega$ ), the probability of moving up a change class is 55%, indicating that negative stream power gradients (high stream power to low) tend to result in geomorphic change. Observations of sediment deposition in reaches with negative stream power gradient indicate that aggradational responses are playing a role in channel change. Finally, a transition from confined to unconfined results in a 70% probability of moving up in response class, indicating that unconfined reaches directly downstream of narrower valleys are relatively susceptible to geomorphic change.

5. Discussion

The Colorado Front Range flood impacted streams along a substantial extent of the foothills and high plains in September 2013, from Fort Collins south to Pueblo. Infrastructure, homes, businesses, stream functions, and ecosystem services were disturbed by the flooding and negatively impacted by emergency response measures within the riparian corridors. Owing to the large spatial extent of flooding induced from this event, from narrow foothill valleys to wide high plains stream corridors, watershed contributing areas ranging from just a few km<sup>2</sup> to >2000 km<sup>2</sup>, and channel slopes from 0.2 to 10%, a wide range in stream scales and conditions was available for database development and analysis. The database was utilized to identify relationships for comparing the hydraulic characteristics of peak flow and geomorphic change, developing a framework for assessing geomorphic change potential.

5.1. Hydraulic thresholds

The development of hydraulic thresholds (Fig. 7A) to help quantify the threat of geomorphic change was evaluated using a data subset.

**Table 4**  
Cumulative logit model coefficient values and diagnostics.

| Model | Model accuracy (%) | Threshold coefficients <sup>a</sup> |      |                        | Predictor variable coefficient values <i>P</i> -value |           |                 |           |                 |                                  |
|-------|--------------------|-------------------------------------|------|------------------------|---|-----------|-----------------|-----------|-----------------|----------------------------------|
|       |                    | 02 3                                | 03 4 | $\beta_1$ <sup>b</sup> | <i>P</i> -value <sup>c</sup>                          | $\beta_2$ | <i>P</i> -value | $\beta_3$ | <i>P</i> -value | POA <i>P</i> -value <sup>d</sup> |
| 5     | 74                 | 0.97                                | 2.84 | 1.66E-04               | <2.2e-16  | -8.33E-05 | 1.68E-06        | -1.77E-06 | 3.40E-07        | 0.02                             |
| 6     | 70                 | 0.61                                | 2.24 | 4.43E-03               | <2.2e-16  | 8.69E-01  | 1.12E-03        | -1.69E-03 | 8.34E-04        | 0.09                             |
| 13    | 81                 | 1.92                                |      | 1.20E-04               | <2.2e-16  | -1.42E-06 | 6.43E-05        |           |                 | n/a                              |
| 15    | 83                 | 1.86                                |      | 1.03E-04               | <2.2e-16  |           |                 |           |                 | n/a                              |
| 15    | 75                 | 0.42                                |      | 1.57E-03               | <2.2e-16  |           |                 |           |                 | n/a                              |

<sup>a</sup> Cumulative logit model threshold coefficient values demarking cumulative logit threshold(s) between categories.

<sup>b</sup> Model parameter coefficient logit values reported in same order as 'Predictor Variable' column in Table 3.

<sup>c</sup> Probability of coefficient being zero based on likelihood ratio test.

<sup>d</sup> Probability associated with likelihood ratio between fixed and unfixed threshold intercept values. Larger probability values indicate that proportional odds assumption of cumulative logit models holds. Lowest *P*-value associated with the parameter that results in largest divergence from proportional odds assumption. Models with two response categories are not applicable to this type of analysis.

To accommodate a precautionary approach to management and design, the 10th and 90th percentiles of  $\omega$  associated with a particular category of channel change (Figs. 5C and 7B) were used to respectively describe that substantial geomorphic change had credible potential or was very likely. Credible potential refers to 10% of the class 4 reaches having  $\omega < 230 \text{ W/m}^2$  and 10% of the class 5 reaches having  $\omega < 480 \text{ W/m}^2$  (excluding depositional-related instability), and very likely refers to 90% of the combined classes 2 and 3 having  $\omega < 700 \text{ W/m}^2$  (Fig. 7B). Hence, stream channels with <3% slope had a credible potential for channel widening where  $\omega$  is  $>230 \text{ W/m}^2$ , and a credible potential for avulsions or braiding (caused by erosion-dominated processes) and loss of adjacent roadway embankments with  $\omega > 480 \text{ W/m}^2$ . Whereas infrequent to numerous eroded banks was very likely with  $\omega > 700 \text{ W/m}^2$ , with substantial channel widening or major geomorphic change shifting from credible to likely. These results generally support the threshold proposed by Magilligan (1992) and provide additional resolution through the use of categorical descriptors of geomorphic change, a larger and more hydraulically diverse study area, and greater remote sensing data availability.

Importantly, these thresholds are based on observations collected in a single semiarid region on stream channels with slopes < 3% and exclude reaches where sediment deposition associated with rapid reductions in stream power dramatically reduced sediment transport capacity and forced geomorphic change at lower levels of power. The extent to which these thresholds are applicable outside of the spatial extent of this analysis is unknown. Stream corridors of the Front Range

foothills and high plains receive average annual precipitation ranging from 380 to 560 mm (Table 2). More humid areas may have different thresholds for geomorphic change, mediated by bed material size, bank material cohesion, and riparian vegetation characteristics. Bias may have also been induced within this data set by excluding reaches obscured by well-vegetated riparian zones where pre-flood leaf-off imagery and LiDAR DEM data sets were unavailable, making a geomorphic change determination untenable. This occurred primarily in smaller headwater reaches. Additionally, because unit stream power at peak flow is the basis of this analysis, the most appropriate geometry for computations was likely somewhere between pre- and post-flood geometry. It is unknown how the use of post-flood geometry influenced the results.

While Magilligan (1992) suggested a  $300 \text{ W/m}^2$  minimum threshold for 'major morphologic change' using data collected in humid climates and Buraas et al. (2014) reinforced this threshold for channel widening, Buraas et al. also found that the  $300 \text{ W/m}^2$  minimum threshold was exceeded for 99% of their 60-km study reach of the Saxons River (Vermont) but that substantial channel widening occurred for only a small fraction of this length. Estimated values of unit stream power well in excess of  $1000 \text{ W/m}^2$  occurred without detectable changes in width reported in some situations. The results of this study are somewhat similar, as the median peak  $\omega$  of the assessed stream reaches with less geomorphic change (infrequent to numerous eroded streambanks) is  $290 \text{ W/m}^2$ . However, only 10% of the assessed reaches (slope < 3%) that experienced a peak  $\omega$  in excess of  $700 \text{ W/m}^2$  have these lesser

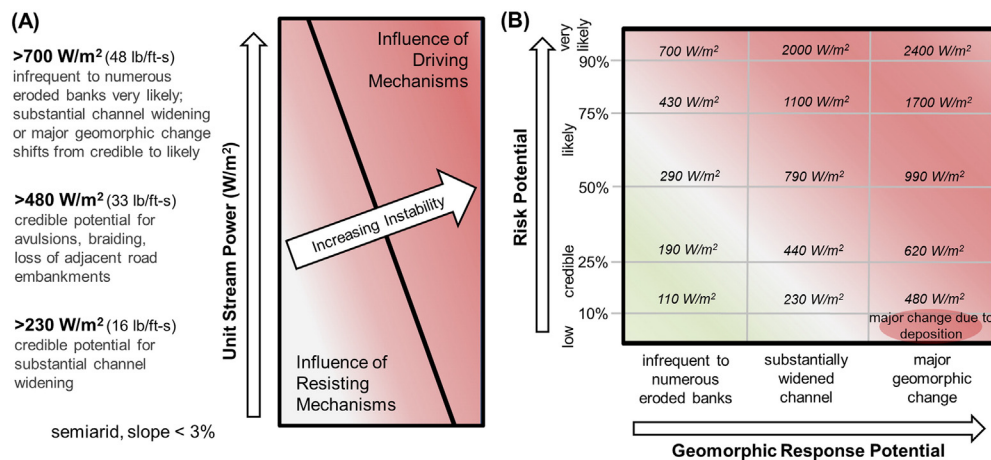


**Fig. 7.** Schematic illustrating conceptual processes and observed thresholds for dominant geomorphic change processes for semiarid streams with slopes < 3% during the 2013 Colorado Front Range flood (A) and a risk potential matrix (based on peak flow  $\omega$ ) for three classes of geomorphic adjustments (B). Driving mechanisms to geomorphic change include discharge, high flow duration, channel and floodplain slope and form, and stream power. Resisting mechanisms to geomorphic change include flow resistance, bank composition, vegetation type and extent, and engineered bank stabilization. The red oval represents stream reaches with major geomorphic change induced by deposition at relatively low  $\omega$ .

amounts of geomorphic change, providing a narrower band of likely expected response. Some of this variability may be caused by this flood having relatively long flood durations.

We observed a shift to lesser geomorphic change at higher unit stream power for channels  $\geq 3\%$ . We hypothesized that mechanistic shifts in geomorphic resistance to change occur as channel slope increases. Increases in channel slope may be associated with larger and more erosion-resistant boundary materials (Baker, 1977; Montgomery and Buffington, 1998). Flow resistance mechanisms also shift as stream gradient increases and bedforms change from riffle-pool and plane bed to step pool and cascade, where bed steps and large roughness elements increase wave drag and force spill resistance from hydraulic jumps, dramatically increasing flow resistance (Lee and Ferguson, 2002; David et al., 2010; Yochum et al., 2012). Large in-channel wood, where present, can also add substantial amounts of flow resistance to channels. This increased flow resistance results in lower reach-average velocities that streambanks must resist to prevent substantial geomorphic adjustments, though large wood can also drive flow into banks and induce local erosion. The slope threshold reflected field observations, the spread of outliers within the data set (Fig. 5A), and a process-based threshold in flow resistance (Montgomery and Buffington, 1997). An implication is that in locations where the longitudinal profile was simplified by grading the channel and removing large clasts as a part of emergency measures to reestablish highway transportation capability after the 2013 flood, the potential for geomorphic and roadway instability may have been exacerbated from the loss of roughness elements, bed armoring, and subsequent flow resistance during future flood events, especially in channels with slopes  $\geq 3\%$ .

For streams with slopes  $\geq 3\%$ ,  $\omega$  increased minimally with increasing geomorphic change (Fig. 5D), which supports the hypothesis that higher-gradient streams respond and adjust to large floods in a different manner. With the majority of streams assessed by Surian et al. (2016) being  $>3\%$ , the result that hydraulic variables alone were not good predictors of geomorphic change may be, in part, owing to variations in bedforms and armoring in their data set and resulting shifts in flow resistance mechanisms. In general, morphological changes in these channels likely reflect many controls occurring at different scales, including site-specific factors such as boundary characteristics, aggradation, and channel curvature (Nardi and Rinaldi, 2015).

The presented thresholds exclude a fundamental mechanism for geomorphic instability: instability induced by abrupt reductions in stream power reducing sediment transport capacity. These step reductions in  $\omega$  result from change in valley form from higher-gradient, confined reaches to lower-gradient, unconfined reaches with substantial floodplains. Owing to the reduction in sediment transport capacity at these locations, deposition of sediment, large wood, and debris within the channels and floodplains was observed to induce geomorphic change for substantial distances downstream.

## 5.2. Valley confinement and longitudinal variation in power

Broader trends in a reduction of  $\omega$  in the downstream direction (Fig. 4) are punctuated by variability resulting from local changes in slopes and channel confinement and significant tributary junctions that result in step changes in width and discharge (Rice et al., 2006). These results in dramatic fluctuations in  $\omega$  associated with changes in slope and valley confinement within the foothills and in the transition from foothills to plains. These fluctuations in  $\omega$  result in fluctuations in channel response in these areas (Fig. 4). For example, a reach confined to a canyon may open up to a wider reach within the canyon where a substantial floodplain exists. Hence, channel confinement by a valley or terrace wall plays an important role in geomorphic change during floods. For a given value of  $\omega$ , greater geomorphic change was observed in unconfined channels. Put another way, smaller values of  $\omega$  often achieved the same geomorphic change classification in unconfined reaches vs. confined reaches, especially for larger-magnitude response classes

(Fig. 6). This contextual relationship between  $\omega$  and geomorphic change can confound attempts to directly relate  $\omega$  to channel response. Our cumulative logit models support this finding. Model coefficient values for predictor variables associated with changes in  $\omega$  and confinement (Table 4) indicate that reductions in  $\omega$ , or negative gradients, and unconfined settings result in increased odds of greater geomorphic change.

The observation that channel confinement by a valley or terrace wall plays an important role in geomorphic change to floods may be explained by two factors. First, confined channels in the study area are generally constrained by highly resistant valley margins composed of either bedrock, hillslope colluvium, or armored roadway embankments (although armored roadway embankments were overwhelmingly eroded along many stream reaches). Second, many of the unconfined reaches are located at the transition from steep confined channels to less steep unconfined channels as the foothills canyons transition to the plains. Additionally, pockets of unconfined reaches embedded within confined reaches exist within the canyons. With the reduction in  $\omega$  occurring within these unconfined reaches, coarse sediment in transport from upstream may have deposited during the floods resulting in more severe channel migration and avulsion at lower levels of  $\omega$ .

Though we did not directly quantify net sediment movement at the reach scale, our observations indicate that erosion of the channel margins (channel widening and incision) drove geomorphic change in confined reaches, whereas a combination of erosion and deposition resulted in channel change in unconfined reaches. More pervasive aggradation within the channels and floodplains as well as channel avulsions were apparent in field observations and DEMs of difference in unconfined reaches, especially in the transition from foothills to plains. As indicated in Figs. 4 and 6, in some places large amounts of geomorphic change were observed in less-confined reaches at lower  $\omega$ . Class 5 reaches with the lowest 10th percentile  $\omega$  values were exclusively of this type. For channels with slopes  $< 3\%$ , the range of this lowest 10th percentile was 86 to 260 W/m<sup>2</sup>, with an average of 170 W/m<sup>2</sup>. These unconfined reaches are typically located downstream of the canyons of the foothills and within the plains downstream of the foothills. Stream power gradient and change in  $\omega$  variables were significant in the cumulative logit models (Table 4) indicating that reductions in  $\omega$  between up- and downstream reaches tends to increase geomorphic response to floods. Though this result reflects a more local-scale influence over 500 to 1000 m, our observations indicate that the influence of this reduction in  $\omega$  can affect streams for several kilometers downstream. In Fig. 4, channel response remains elevated at categories 4 and 5 well after values of  $\omega$  have decreased in the transition from the foothills to the plains. This elevated change came in the form of channel avulsions and downstream migration of meanders and concomitant aggradation as indicated by the DEMs of difference.

We observed multiple examples of a magnified geomorphic change in unconfined segments downstream of confined segments including the north and south forks of St. Vrain Creek in Lyons as well as the confluence of the north fork with the mainstem Big Thompson River in Drake. This may be caused by a transition from erosion-dominated geomorphic to deposition-dominated change as sediment transport capacities generally decrease in the downstream direction (Schumm, 1977; Montgomery and Buffington, 1997; Church, 2002;). Bizzi and Lerner (2013) found that  $\Omega$  averaged over 3- to 5-km upstream segments was the best predictor of whether a channel was erosional or depositional. Similarly, Gartner et al. (2015) found that negative  $\Delta\Omega/\Delta x$ , calculated from a moving average with a window ranging from 200 to 1000 m, corresponded well with erosional responses to floods and that a positive gradient corresponded well with aggradational responses. Where our data extended from the foothills well onto the plains (St. Vrain Creek, Left Hand Creek, Coal Creek), we observed major geomorphic change (categories 4 and 5) for 10–15 km downstream of dramatic drops in  $\omega$  at the transition from the foothills to the plains (Fig. 4). Geomorphic change to floods, therefore, is not only

driven by the physical properties within a given reach but also the position of that reach relative to other reaches. Future studies that examine scaling of an upstream analysis domain based on drainage area, channel width, or other factors may reveal longitudinal patterns of decreasing flood power associated with significant channel responses to sediment deposition.

### 5.3. Contextual geomorphic change mechanisms

Variable driving and resisting mechanisms for geomorphic change were observed from aerial imagery, LiDAR elevation data, and on-the-ground site visits. Driving mechanisms include stream power, variations in sediment and debris availability for transport (including landslides and debris flows), and localized flow variability. Resisting mechanisms include bed and streambank material composition, riparian vegetation composition and extent, high flow resistance (limiting streamflow velocity), and engineered bank stabilization (riprap, retaining walls, etc.). Hence, variability in driving and resisting mechanisms that were present within each reach added variability in the geomorphic response.

While we did not emphasize the role of engineering bank stabilization in this study, we did note that rip rap and other engineering bank stabilization measures were intermittently present (and visible in aerial imagery) on many of the evaluated reaches prior to the flooding. Many of the embankments protected by rip rap failed and the reaches experienced major geomorphic change (classes 4 and 5), especially in reaches with higher  $\omega$  and on the outside of meander bends (e.g., Big Thompson). Other reaches with rip rap only experienced infrequent to numerous eroded streambanks (classes 2 and 3), especially on the Cache la Poudre (where the flood was less severe, the stream is less confined, and lower  $\omega$  experienced).

Increased geomorphic change was, in places, observed immediately downstream of landslides and debris flows that occurred on adjacent upland slopes; observation of this include upper portions of the Big Thompson River and South St. Vrain Creek. This phenomenon has been previously noted (Cenderelli and Kite, 1998). Mechanistically, this is reasonable as the specific weight of the fluid can substantially change in sediment-laden water, with the specific weight as much as doubling in some circumstances as the flow shifts from being a water flood, to hyperconcentrated flow, to a debris flow (Costa, 1988). Doubling the specific weight would double the  $\omega$  (with subsequent increased potential for geomorphic work), though additional mechanistic changes also occur as sediment concentration increases, including changes in shear strength, viscosity, and particle fall velocity and with a fundamental shift in sediment transport from water and solids moving as separate components (water floods, hyperconcentrated flows), to particles and water moving together as a single body (debris flows).

Additionally, increased geomorphic change was also observed downstream of local and river segment scale flow transitions, such as overly restrictive bridge openings (e.g., private bridges on Big Thompson River and Buckhorn Creek) and transitions from confined to unconfined reaches. Locally dominating two- and three-dimensional flow patterns can induce local erosion that subsequently unravels reach-scale streambanks and floodplains, with potential for impacting infrastructure, homes, and businesses for a substantial downstream extent. This effect has also been noted by others; as an example, Hajdukiewicz et al. (2016) noted for a flood in Poland that width restrictions at bridges resulted in insufficient flow conveyance and bridge failures.

### 5.4. Application

The cumulative logit modeling provides a reasonable statistical framework for (i) characterizing the relative importance of different hydraulic and geomorphic variables on channel response, and (ii) predicting channel response elsewhere a priori based on a model

calibrated from a regional database. One of the above models could be applied elsewhere in and along the Colorado Front Range, for instance, using a geodatabase of reach-scale flood discharge, slope, and confinement to predict categorical channel response for a specified flood frequency (e.g., the 100-year flood).

The  $\omega$  thresholds for differing classes of geomorphic change may also have applicability in identifying fluvial hazards and evaluating the susceptibility of proposed projects within stream corridors. Practitioners currently need quantitative tools to more rigorously analyze and assess stream corridor designs. Although this study is based upon a single semiarid region, the results can be utilized with caution to provide a quantification tool in this and potentially other semi-arid regions. To illustrate the potential value, a hypothetical application is described below.

Consider a highway realignment project being designed in a semiarid riparian setting in western North America. The stream has an average slope of 1.8%, is semiconfined, and has varying floodplain widths between a steep valley wall and an existing 2-lane state highway. The roadway is planned to be expanded from 2 to 4 lanes. The initial design would further constrain the riparian zone by filling the valley bottom for the expanded roadway and associated features. Thus, there is concern that this design could result in a highway corridor that is substantially more susceptible to geomorphic failure and riparian impacts during large floods.

One-dimensional, gradually varied, steady state hydraulic models were developed in HEC-RAS for existing and proposed conditions for the 100-year flood. The modeling results show longitudinal variability in  $\omega$  throughout the project reach and between existing and proposed conditions; however, there are no dramatic longitudinal decreases in  $\omega$  that indicate a potential for depositional-induced geomorphic instability (bottom right corner of Fig. 7B). Hence, the technical team focuses on the potential for erosion-induced instability of the proposed conditions. Modeling indicates that the proposed conditions will, on average, increase  $\omega$  from 190 to 280 W/m<sup>2</sup>, with some proposed locations experiencing  $\omega$  of 550 W/m<sup>2</sup> and one location where  $\omega$  is estimated at 760 W/m<sup>2</sup> during the 100-year flood.

Using the thresholds provided in Fig. 7A and a precautionary approach, it is noted that the proposed conditions have, on average, a credible potential for channel widening and, in some locations, a credible potential for avulsions and the loss of road embankment. At one location it is likely that a portion of the roadway embankment could likely be lost during large floods. Using the matrix provided in Fig. 7B, it is indicated that the one location where  $\omega$  is estimated at 760 W/m<sup>2</sup> is of special concern since, during the 2013 Colorado Front Range Flood, infrequent to numerous eroded banks were very likely, and a substantially widened channel or major geomorphic change were shifting from credible to likely. Locations where  $\omega$  reaches 550 W/m<sup>2</sup> represent additional primary points of concern to roadway stability, and a general increase in  $\omega$  to 280 W/m<sup>2</sup> indicates an increased potential for channel widening and, hence, a possible threat to riparian conditions.

## 6. Summary and conclusions

This study has utilized an extensive data set from the 2013 Colorado Front Range Flood to relate channel adjustments to descriptors of driving processes and geomorphic setting. We defined six classes of geomorphic change related to stream power and valley confinement for 531 stream reaches over 226 km, spanning a gradient of channel scales, slopes, and watershed areas. The geomorphic change classes (and median  $\omega$  values) were: (1) no detected geomorphic change; (2) infrequent eroded streambanks (280 W/m<sup>2</sup>); (3) numerous eroded streambanks (370 W/m<sup>2</sup>); (4) a substantially widened channel over the majority of the reach length (970 W/m<sup>2</sup>); (5) major geomorphic changes, with avulsions, braiding, or roadway embankments and high terraces eliminated or substantially eroded by erosional and/or depositional processes (1100 W/m<sup>2</sup>); and (6) narrow valley form (canyon) limits

geomorphic change potential, with no substantial pre-flood floodplains detected ( $3900 \text{ W/m}^2$ ). Unit stream power has a positive relationship to the geomorphic change classification, and greater geomorphic change was observed in unconfined compared to confined channels for a given value of  $\omega$ . Stratification of the data set revealed  $\omega$  thresholds and shifts in resisting mechanisms to geomorphic change as slope increases from changes in channel type, bedforms, flow resistance and bed armoring potential, as well as a differing mechanism for major geomorphic change resulting from large reductions in stream power and deposition.

The results of these analyses have the potential for direct applicability to the management of stream corridors. The key findings of this study are as follows:

- We noted a relatively strong direct relationship between peak flow unit stream power ( $\omega$ ) and magnitudes of geomorphic change experienced during the 2013 Colorado Front Range flood.
- For channel slopes  $< 3\%$  in this semiarid landscape, we noted a credible potential for substantial channel widening with  $\omega > 230 \text{ W/m}^2$  (10% of the observed adjustment class reaches had  $\omega < 230 \text{ W/m}^2$ ); a credible potential for avulsions, braiding, and loss of adjacent road embankments with  $\omega > 480 \text{ W/m}^2$ ; and with  $\omega > 700 \text{ W/m}^2$  infrequent to numerous eroded banks were very likely (90% of the observed adjustment class reaches had  $\omega < 700 \text{ W/m}^2$ ) and the risk of substantial channel widening or major geomorphic change shifts from credible to likely. These thresholds can be utilized for assessing the geomorphic hazard potential via hydraulic modeling.
- Channels with slopes  $> 3\%$  resisted geomorphic change at higher  $\omega$ , likely because of bed armoring and enhanced flow resistance induced from bedform flow dynamics forced by large clasts and, where available, large instream wood.
- Channel instability induced from deposition resulted in major reach-scale geomorphic change at relatively low  $\omega$  at some locations, on average about  $170 \text{ W/m}^2$  and as low as  $86 \text{ W/m}^2$ . This was observed in lower-gradient, unconfined reaches downstream of confined and steeper reaches. This effect can result in elevated geomorphic change for several kilometers downstream.
- Cumulative logit modeling indicated that stream power or unit stream power, unit stream power gradient, and valley confinement are valuable for predicting the geomorphic change. Models that included terms representing all of these variables performed well in differentiating among multiple geomorphic change categories. A single predictor model based on stream power performed well in predicting a binary channel response variable (moderate vs. major change).

These results indicate that using  $\omega$  thresholds for estimating expected future adjustments of stream channels within and along the Colorado Front Range during floods is reasonable in channels with slopes  $< 3\%$ , though it needs to be understood that there is still a potential for large amounts of geomorphic change below these thresholds along streams where stream power substantially and abruptly decreases. These results may also be applicable to streams in other semiarid landscapes, especially regions where mountain channel types spanning a similar range of slopes are affected by mixed snowmelt and monsoonal hydroclimatology.

Further research is needed to assess the potential broader applicability of these thresholds and to develop better understanding of geomorphic change to be expected during large floods. The influence of flood duration, which likely contributed to the magnitude of impacts, was not assessed because of the loss of streamflow gages during the flooding, as well as the lack of streamflow gages in headwater streams within the foothills. Greater understanding of the role of flood duration in geomorphic change is needed. Improved understanding of major geomorphic change induced at relatively low local  $\omega$  within the context of the negative longitudinal stream power gradients and changes in channel confinement is also needed. Additional research on the

mechanisms behind the relatively greater and more variable range of  $\omega$  associated with geomorphic change in stream channels with slopes  $> 3\%$  would be a valuable pursuit. Finally, additional understanding of the role of local lithological and topographic controls as well as role of significant tributaries, landslides and debris flows, and restrictive bridge openings on geomorphic change induced during large floods is needed.

## Acknowledgements

We thank Sara Rathburn and John Moody, as well as an anonymous reviewer, for constructive reviews that substantially improved the manuscript. Additional review and editorial work by Richard Marston, Gene Bosley, and David Levinson is also greatly appreciated.

The many hydrologists and hydraulic engineers who collected the peak flow data utilized in this analysis are greatly appreciated. This includes individuals with the U.S. Geological Survey and the Colorado Division of Water Resources, for peak flow estimates as well as the routine stream gaging efforts that provided the annual peak flow data required to perform the flood frequency analyses. John Moody (USGS), Bob Jarrett (retired USGS), and Dan Moore (NRCS) are explicitly recognized for their work with developing peak flow estimates.

Joel Sholtes and Brian Bledsoe gratefully acknowledge support from the Colorado Water Institute and the Colorado Water Conservation Board.

## Appendix A. Supplementary data

Supplementary data associated with this article can be found in the version, at doi: [10.1016/j.geomorph.2017.03.004](https://doi.org/10.1016/j.geomorph.2017.03.004). These data include a Google Earth file with the analyzed reaches and results.

## References

- Aguilar, J., 2014. Colorado re-emerging from \$2.9 billion flood disaster a year later. *Denver Post* Sept. 6, 2014.
- American Association of Floodplain Managers (ASFPM), 2016. Riverine Erosion Hazards White Paper. (Madison WI. 48p. <http://www.floods.org/ace-images/ASFPMRiverineErosionWhitePaperFeb2016.pdf>).
- Anderson, S.W., Anderson, S.P., Anderson, R.S., 2015. Exhumation by debris flows in the 2013 Colorado Front Range storm. *Geology* 43 (5):391. <http://dx.doi.org/10.1130/G36507.1>.
- Baker, V.R., 1977. Stream-channel response to floods, with examples from central Texas. *Geol. Soc. Am. Bull.* 88 (8), 1057–1071.
- Baker, V.R., Costa, J.E., 1987. Flood power. In: Mayer, L., Nash, D. (Eds.), *Catastrophic Flooding*. Allen and Unwin, Boston, pp. 1–21.
- Benito, G., 1997. Energy expenditure and geomorphic work of the cataclysmic Missoula flooding in the Columbia River Gorge, USA. *Earth Surf. Process. Landf.* 22, 457–472.
- Biron, P.M., Buffin-Belanger, T., Larocque, M., Chone, G., Cloutier, C., Ouellet, M., Demers, S., Olsen, T., Desjarlais, C., Eyquem, J., 2014. Freedom space for rivers: a sustainable management approach to enhance river resilience. *Environ. Manag.* 54:1056–1073. <http://dx.doi.org/10.1007/s00267-014-0366-z>.
- Bizzi, S., Lerner, D.N., 2013. The use of stream power as an indicator of channel sensitivity to erosion and deposition processes. *River Res. Appl.* <http://dx.doi.org/10.1002/rra.2717>.
- Bodhaine, G.L., 1968. Measurement of peak discharge at culverts by indirect methods. *U.S. Geological Survey Techniques of Water-Resources Investigations (Book 3, chap. A3, 48 p)*.
- Brooks, G.R., Lawrence, D.E., 1999. The drainage of the Lake Ha!Ha! reservoir and downstream geomorphic impacts along Ha!Ha! River, Saguenay area, Quebec, Canada. *Geomorphology* 28, 141–168.
- Bull, W.B., 1979. Threshold of critical power in streams. *Geol. Soc. Am. Bull.* 90, 453–464 Part I.
- Buraas, E.M., Renshaw, C.E., Magilligan, F.J., Dade, W.B., 2014. Impact of reach geometry on stream channel sensitivity to extreme floods. *Earth Surf. Process. Landf.* 39: 1778–1789. <http://dx.doi.org/10.1002/esp.3562>.
- Carlson, E.A., 2009. Fluvial riparian classification for National Forests in the Western United States. Master's Thesis. Colorado State University, Fort Collins, CO.
- Cenderelli, D.A., Kite, J.S., 1998. Geomorphic effects of large debris flows on channel morphology at North Fork Mountain, Eastern West Virginia. *Earth Surf. Process. Landf.* 23, 1–19.
- Cenderelli, D.A., Wohl, E.E., 2003. Flow hydraulics and geomorphic effects of glacial-lake outburst floods in the Mount Everest region, Nepal. *Earth Surf. Process. Landf.* 28, 385–407.
- Christensen, R.H.B., 2015a. A Tutorial on Fitting Cumulative Link Models with the Ordinal Package. <http://www.cran.r-project.org/package=ordinal/>.

- Christensen, R.H.B., 2015b. Ordinal — Regression Models for Ordinal Data. R Package Version. 2015:pp. 6–28. <http://www.cran.r-project.org/package=ordinal/>.
- Church, M., 2002. Geomorphic thresholds in riverine landscapes. *Freshw. Biol.* 47 (4), 541–557.
- Coe, J.A., Kean, J.W., Godt, J.W., Baum, R.L., Jones, E.S., Gochis, D.J., Anderson, G.S., 2014. New insights into debris-flow hazards from an extraordinary event in the Colorado Front Range. *GSA Today* 24 (10). <http://dx.doi.org/10.1130/GSATG214A.1>.
- Community Collaborative Rain, Hail & Snow Network (CoCoRaHS) 2013. Data accessed 9/13/2013. <http://www.cocorahs.org/ViewData/>.
- Core Team, R., 2015. R: A Language and Environment for Statistical Computing. R Foundation for Statistical Computing, Vienna, Austria (URL <https://www.R-project.org/>).
- Costa, J.E., 1988. Rheologic, geomorphic, and sedimentologic differentiation of water flows, hyperconcentrated flows, and debris flows. In: Baker, V.R., Kochel, R.C., Patton, P.C. (Eds.), *Flood Geomorphology*, N.Y. John Wiley and Sons.
- Costa, J.E., O'Connor, J.E., 1995. Geomorphically effective floods. In: Costa, J.E., Miller, A.J., Potter, K.W., Wilcock, P.R. (Eds.), *Natural and Anthropogenic Influences in Fluvial Geomorphology*. 89. American Geophysical Union, Geophysical Monograph, pp. 45–56.
- Cunnean, C., 1978. Unbiased plotting positions — a review. *J. Hydrol.* 37 (Issue 3):205–222. ISSN 0022-1694. [10.1016/0022-1694\(78\)90017-3](http://dx.doi.org/10.1016/0022-1694(78)90017-3).
- Dalrymple, T., Benson, M.A., 1968. Measurement of peak discharge by the slope-area method. U.S. Geological Survey Techniques of Water-Resources Investigations (Book 3, chap. A2, 12 p).
- Daly, C., Halbleib, M., Smith, J.L., Gibson, W.P., Doggett, M.K., Taylor, G.H., Curtis, J., Pasteris, P.A., 2008. Physiographically-sensitive mapping of temperature and precipitation across the conterminous United States. *Int. J. Climatol.* 28, 2031–2064.
- David, G.C.L., Wohl, E., Yochum, S.E., Bledsoe, B.P., 2010. Controls on spatial variations in flow resistance along steep mountain streams. *Water Resour. Res.* 46, W03513. <http://dx.doi.org/10.1029/2009WR008134>.
- Dunn, O.J., 1961. Multiple comparisons among means. *J. Am. Stat. Assoc.* 56 (293), 52–64.
- Ferencevic, M.V., Ashmore, P., 2012. Creating and evaluating digital elevation model-based stream-power map as a stream assessment tool. *River Res. Appl.* 28: 1394–1416. <http://dx.doi.org/10.1002/rra.1523>.
- Fuller, I.C., 2008. Geomorphic impacts of a 100-year flood: Kiwitea Stream, Manawatu catchment, New Zealand. *Geomorphology* 98:84–95. <http://dx.doi.org/10.1016/j.geomorph.2007.02.026>.
- Gartner, J.D., Dade, W.B., Renshaw, C.E., Magilligan, F.J., Buraas, E.M., 2015. Gradients in stream power influence lateral and downstream sediment flux in floods. *Geology* <http://dx.doi.org/10.1130/G36969.1>.
- Gochis, D., Schumacher, R., Friedrich, K., Doesken, N., Kelsch, M., Sun, J., Ikeda, K., Lindsey, D., Wood, D., Dolan, B., Matrosow, S., Newman, A., Mahoney, K., Rutledge, S., Johnson, R., Kucera, P., Kennedy, P., Sempere-Torres, D., Steiner, M., Roberts, R., Wilson, J., Yu, W., Chandrasekar, V., Rasmussen, R., Anderson, A., Brown, B., 2015. The Great Colorado Flood of September 2013. *Bull. Am. Meteorol. Soc.* 96, 1461–1487.
- Graf, W.L., 1984. A probabilistic approach to the spatial assessment of river channel instability. *Water Resour. Res.* 20 (7), 953–962.
- Hajdukiewicz, H., Wyzga, B., Mikus, P., Zawiejaska, J., Radecki-Pawlik, A., 2016. Impact of a large flood on mountain river habitats, channel morphology, and valley infrastructure. *Geomorphology* 272:55–67. <http://dx.doi.org/10.1016/j.geomorph.2015.09.003>.
- Hauer, C., Habersack, H., 2009. Morphodynamics of a 1000-year flood in the Kamp River, Austria, and impacts on floodplain morphology. *Earth Surf. Process. Landf.* 34: 654–682. <http://dx.doi.org/10.1002/esp.1763>.
- Hooke, J.M., Mant, J.M., 2000. Geomorphological impacts of a flood event on ephemeral channels in SE Spain. *Geomorphology* 34, 163–180.
- Hulsing, H., 1967. Measurement of peak discharge at dams by indirect methods. U.S. Geological Survey Techniques of Water-Resources Investigations (book 3, chap. A5, 29 p).
- Interagency Advisory Committee on Water Data (IACWD), 1982. *Flood Flow Frequency: Bulletin #17B of the Hydrology Subcommittee*. U.S. Department of Interior, Geological Survey, Office of Water Data Coordination.
- Jagt, K., Blazewicz, M., Sholtes, J., 2016. Fluvial hazard zone delineation: a framework for mapping channel migration and erosion hazard areas in Colorado. Prepared for Colorado Water Conservation Board. Department of Natural Resources (Draft 1/14/2016, 69 pp).
- Jarrett, R.D., 2014. Written Communication, Applied Weather Associates.
- Jarrett, R.D., England, J.F., 2002. Reliability of paleostage indicators for paleoflood studies. In: House, P.K., Webb, R.H., Baker, V.R., Levish, D.R. (Eds.), *Ancient Floods, Modern Hazards: Principles and Applications of Paleoflood Hydrology*. Vol. 5. American Geophysical Union, Water Science and Application, pp. 91–109.
- Jarrett, R.D., Tomlinson, E.M., 2000. Regional interdisciplinary paleoflood approach to assess extreme flood potential. *Water Resour. Res.* 23 (10), 2957–2984.
- Kale, V.S., 2003. Geomorphic effects of monsoon floods on Indian rivers. *Nat. Hazards* 28, 65–84.
- Kimbrough, R.A., Holmes, R.R., 2015. Flooding in the South Platte River and Fountain Creek Basins in Eastern Colorado, September 9–18, 2013. U.S. Department of Interior, U.S. Geological Survey, Scientific Investigations Report 2015–5119.
- Krapesch, G., Hauer, C., Habersack, H., 2011. Scale orientated analysis of river width changes due to extreme flood hazards. *Nat. Hazards Earth Syst. Sci.* 11:2137–2147. <http://dx.doi.org/10.5194/nhess-11-2137-2011>.
- Kruskal, W., Wallis, W.A., 1952. Use of ranks in one-criterion variance analysis. *J. Am. Stat. Assoc.* 47 (260):583–621. <http://dx.doi.org/10.1080/01621459.1952.10483441>.
- Lane, S.N., Westaway, R.M., Murray Hicks, D., 2003. Estimation of erosion and deposition volumes in a large, gravel-bed, braided river using synoptic remote sensing. *Earth Surf. Process. Landf.* 28 (3), 249–271.
- Lea, D.M., Legleiter, C.J., 2015. Mapping the spatial patterns of stream power and channel change along a gravel-bed river in northern Yellowstone. *Geomorphology* <http://dx.doi.org/10.1016/j.geomorph.2015.05.033>.
- Lee, A.J., Ferguson, R.I., 2002. Velocity and flow resistance in step-pool streams. *Geomorphology* 46, 59–71.
- Magilligan, F.J., 1992. Thresholds and the spatial variability of flood power during extreme floods. *Geomorphology* 5, 373–390.
- Magilligan, F.J., Buraas, E.M., Renshaw, C.E., 2015. The efficacy of stream power and flow duration on geomorphic responses to catastrophic flooding. *Geomorphology* 228: 175–188. <http://dx.doi.org/10.1016/j.geomorph.2014.08.016>.
- Matthai, H.F., 1967. Measurement of peak discharge at width contractions by indirect methods. U.S. Geological Survey Techniques of Water-Resources Investigations (book 3, chap. A4, 44 p).
- McLeod, A.I., 2015. Package 'Kendall'. <https://cran.r-project.org/web/packages/Kendall/index.html>.
- Miller, A.J., 1990. Flood hydrology and geomorphic effectiveness in the Central Appalachians. *Earth Surf. Process. Landf.* 15, 119–134.
- Montgomery, D.R., Buffington, J.M., 1997. Channel reach morphology in mountain drainage basins. *Geol. Soc. Am. Bull.* 109 (5), 596–611.
- Montgomery, D.R., Buffington, J.M., 1998. Channel processes, classification, and response. In: Naiman, R.J., Bilby, R.E. (Eds.), *River Ecology and Management: Lessons from the Pacific Coastal Ecoregion*. Springer-Verlag, New York, New York, pp. 13–42.
- Moody, J.A., 2016. Estimates of peak discharge for 21 sites in the Front Range in Colorado in response to extreme rainfall in September 2013. U.S. Geological Survey Scientific Investigations Report 2016–5003 <http://dx.doi.org/10.3133/sir20165003>.
- Nardi, L., Rinaldi, M., 2015. Spatio-temporal patterns of channel changes in response to a major flood event: the case of the Magra River (central-northern Italy). *Earth Surf. Process. Landf.* 40 (3), 326–339.
- National Weather Service, 2013. Exceedance probability analysis for the Colorado Flood Event, 9–16 September 2013. Hydrometeorological Design Studies Center, National Weather Service. National Oceanic and Atmospheric Administration, Bethesda, MD. 5p. [http://www.nws.noaa.gov/oh/hdsc/aep\\_storm\\_analysis/8\\_Colorado\\_2013.pdf](http://www.nws.noaa.gov/oh/hdsc/aep_storm_analysis/8_Colorado_2013.pdf).
- Olson, P.L., Legg, N.T., Abbe, T.B., Reinhart, M.A., Radloff, J.K., 2014. A Methodology for Delineating Planning-level Channel Migration Zones. Washington State Dept. of Ecology, Olympia, WA (83p).
- Ortega, J.A., Heydt, G.G., 2009. Geomorphological and sedimentological analysis of flash-flood deposits: the case of the 1997 Rivillas flood (Spain). *Geomorphology* 112: 1–14. <http://dx.doi.org/10.1016/j.geomorph.2009.05.004>.
- Parker, C., Thorne, C.R., Clifford, N.J., 2015. Development of ST:REAM: a reach-based stream power balance approach for predicting alluvial river channel adjustment. *Earth Surf. Process. Landf.* 40:403–413. <http://dx.doi.org/10.1002/esp.3641>.
- Piegay, H., Darby, S.E., Mosselman, E., Surian, N., 2005. A review of techniques available for delimiting the erodible river corridor: a sustainable approach to managing bank erosion. *River Res. Appl.* 21, 773–789.
- Rathburn, S., Bennett, G., Wohl, E., Briles, C., McElroy, B., Sutfin, N., 2017. The fate of sediment, wood and organic carbon eroded during an extreme flood, Colorado Front Range, USA. *Geology* <http://dx.doi.org/10.1130/G38935.1>.
- Rice, S.P., Ferguson, R.I., Hoey, T.B., 2006. Tributary control of physical heterogeneity and biological diversity at river confluences. *Can. J. Fish. Aquat. Sci.* 63 (11), 2553–2566.
- Schram, H., Wulliman, J.T., Rapp, D.N., 2014. Hydrologic evaluation of the St. Vrain watershed: post September 2013 flood event. Prepared for the Colorado Department of Transportation, Region 4 Flood Recovery Office, Jacobs Engineering, Denver, Colorado.
- Schumm, S.A., 1977. *The Fluvial System*. Wiley-Interscience, New York (338pp).
- Surian, N., Righini, M., Lucia, A., Nardi, L., Amponsah, W., Benvenuti, M., Borga, M., Cavalli, M., Comiti, F., Marchi, L., Rinaldi, M., Viero, A., 2016. Channel response to extreme floods: insights on controlling factors from six mountain rivers in northern Apennines, Italy. *Geomorphology* <http://dx.doi.org/10.1016/j.geomorph.2016.02.002>.
- Thompson, C., Croke, J., 2013. Geomorphic effects, flood power, and channel competence of a catastrophic flood in confined and unconfined reaches of the upper Lockyer valley, southeast Queensland, Australia. *Geomorphology* 197:156–169. <http://dx.doi.org/10.1016/j.geomorph.2013.05.006>.
- Tye, M.R., Cooley, D., 2015. A spatial model to examine rainfall extremes in Colorado's Front Range. *J. Hydrol.* 530:15–23. <http://dx.doi.org/10.1016/j.jhydrol.2015.09.023>.
- Urban Drainage and Flood Control District. (UDFCD), 2014. 2013 Flood Peak Estimates. (Data accessed 7/14/2014. <http://udfcd.maps.arcgis.com/home/gallery.html>).
- Webb, R.H., Jarrett, R.D., 2002. One-dimensional estimation techniques for discharges of paleofloods and historical floods. In: House, P.K., Webb, R.H., Baker, V.R., Levish, D.R. (Eds.), *Ancient Floods, Modern Hazards: Principles and Applications of Paleoflood Hydrology*. Vol. 5. American Geophysical Union, Water Science and Application, pp. 111–125.
- Wheaton, J.M., Brasington, J., Darby, S.E., Sear, D.A., 2010. Accounting for uncertainty in DEMs from repeat topographic surveys: improved sediment budgets. *Earth Surf. Process. Landf.* 35 (2), 136–156.
- Wohl, E., 2010. A brief review of the process domain concept and its application to quantifying sediment dynamics in bedrock canyons. *Terra Nova* 22 (6), 411–416.
- Yochum, S.E., 2015. Colorado Front Range Flood of 2013: peak flows and flood frequencies. Proceedings from the 3rd Joint Federal Interagency Conference on Sedimentation and Hydrologic Modeling, April 19–23, 2015, Reno, Nevada, USA.
- Yochum, S.E., Moore, D.S., 2013. Colorado Front Range Flood of 2013: Peak Flow Estimates at Selected Mountain Stream Locations. U.S. Department of Agriculture, Natural Resources Conservation Service, Colorado State Office.
- Yochum, S.E., Goertz, L.A., Jones, P.H., 2008. Case study of the big bay dam failure: accuracy and comparison of breach predictions. *J. Hydraul. Eng.* 134 (9). [http://dx.doi.org/10.1061/\(ASCE\)0733-9429\(2008\)134:9\(1285\)](http://dx.doi.org/10.1061/(ASCE)0733-9429(2008)134:9(1285)).
- Yochum, S.E., Bledsoe, B.P., David, G.C.L., Wohl, E., 2012. Velocity prediction in high-gradient channels. *J. Hydrol.* <http://dx.doi.org/10.1016/j.jhydrol.2011.12.031>.
- Yochum, S.E., Comiti, F., Wohl, E., David, G.C.L., Mao, L., 2014. Photographic guidance for selecting flow resistance coefficients in high-gradient channels. U.S. Department of Agriculture, Forest Service, Rocky Mountain Research Station, General Technical Report RMRS-GTR-323.